Accepted Manuscript

Title: Curvature development in Ring Rolling

Authors: Christopher J. Cleaver, Julian M. Allwood

PII: S0924-0136(18)30559-4
DOI: https://doi.org/10.1016/j.jmatprotec.2018.12.025
Reference: PROTEC 16064

To appear in: *Journal of Materials Processing Technology*

Received date: 13 June 2018
Revised date: 11 October 2018
Accepted date: 14 December 2018

Please cite this article as: Cleaver CJ, Allwood JM, Curvature development in Ring Rolling, *Journal of Materials Processing Tech.* (2018), https://doi.org/10.1016/j.jmatprotec.2018.12.025

Curvature development in Ring Rolling

Christopher J. Cleaver*[a]

Julian M. Allwood[a]

a. Department of Engineering, University of Cambridge, Trumpington Street, Cambridge, CB2 1PZ

* Corresponding author cjc82@cam.ac.uk

Abstract

Loss of circularity when creating metal ring-shaped products by ring rolling is a significant industrial issue. This paper explores the previously tacit knowledge that plastic changes in curvature - required to maintain circularity - principally occur as material passes through the roll gap. Through a series of experiments and numerical simulations on half-ring workpieces, the 'free curvature change' is explored for the first time, finding that the ring can 'curl up' - the radius reducing by as much as -39% in a single pass - unless the inner roll is much smaller than the outer roll. An analytical model of free curvature change is proposed based on force equilibrium and compatibility. Under a range of 'normal' operating conditions this predicted free curvature change to within 7%. In (full) ring rolling the radius of curvature must continually increase. This paper proposes that regulation of curvature is achieved through bending moments at the roll entry and exit; largest when the tool size ratio is furthest from the optimum. This hypothesis is supported by Finite Element simulations of full ring rolling, finding entry and exit moments up to a quarter of the moment for a fully plastic hinge. This work could be of direct use to process designers in choosing tool sizes and guide roll force limits and suggests new ways to use guide rolls to better maintain circularity in challenging situations.

Keywords

Ring rolling; Curvature; Analytical modelling

1 Introduction

Ring rolling is a forming process for making seamless semi-finished metal ring products. These are used in annular components prevalent in engineering applications such as aero engines, energy turbines and industrial pipework. In 2016 9% of forged products by weight recorded worldwide were seamless rings (Euro Forge, 2018).

In the radial ring rolling process (Fig 1a) a thinner walled ring is produced from a pierced preform. The preform is rolled between a pair of tools acting on the inner and outer radial surfaces; the outer tool, known as the forming roll, is powered to rotate, while the idly rotating inner tool – the mandrel - translates to incrementally reduce the ring wall thickness. As a result of this reduction in thickness - in the region of 1-10% per revolution- the ring's circumferential length increases and its radius of curvature in the x-y plane consequently increases.

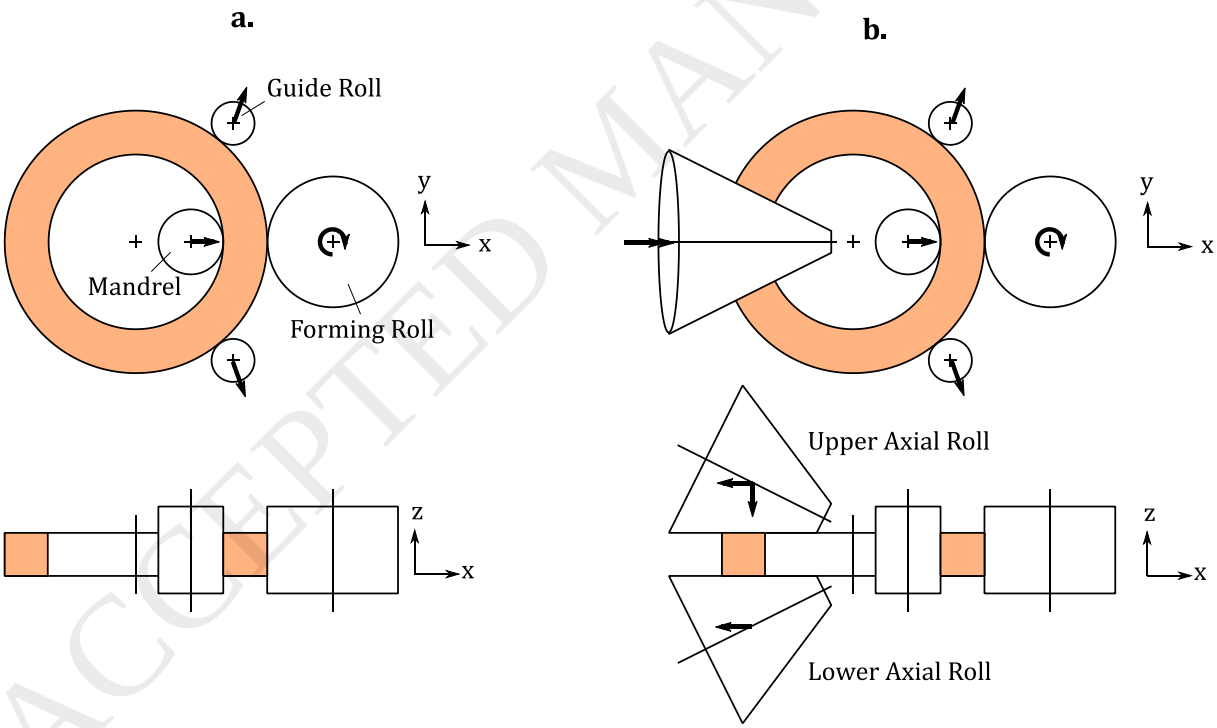

Fig 1 Process set-up for **a.** radial ring rolling **b.** radial-axial ring rolling

To ensure that overall circularity remains within acceptable limits, two 'guide rolls' are commonly used. These are positioned on the outside of the ring either side of the radial roll

zone, as shown in Fig 1. They are moved in such a way that they both centre the ring in the y direction, and accommodate increases in radius. A number of control strategies for these guide rolls have been discussed in the literature, including force controlled approaches (e.g. Li et. al., 2008), and active closed-loop position control (e.g. Jenkouk et. al., 2012).

Whichever route is used the degree of circularity achievable may not meet the tolerance demanded in the final product specification, and so either extra material must be added to ensure the final part can be machined and/or the circularity can be improved by using an additional processing stage after ring rolling – ring expansion - (Fig 2). In this, the ring is stretched by a set of tools that simultaneously move radially outwards.

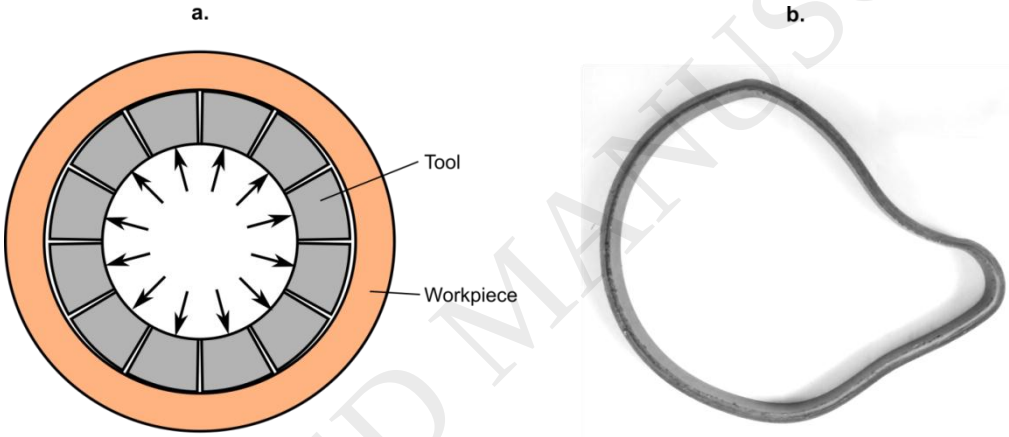

Fig 2 a. Ring expander **b.** Complete loss of circularity in ring rolling (Cleaver, 2016)

Avoiding complete loss of circularity– such as Fig 2b - is a significant challenge especially when rolling highly thin-walled rings. Gellhaus (1999) defines a parameter, P, the 'Eigen Stiffness' of a ring to indicate how difficult it is to ring roll. He argues that to successfully roll thin, compliant, rings very careful consideration of the tool kinematics is required.

Despite this significant industrial challenge, relatively little is known about the mechanics of how curvature – and hence circularity - develops during ring rolling. A brief review is now provided.

1.1 Literature on curvature change mechanics in Ring Rolling

In ring rolling, the process controller typically targets a smooth *average* radius growth rate profile such as in Fig 3. However, intuition suggests it is highly unlikely the curvature about a *given material point* in the ring will uniformly increase in this way. To do so, the curvature would continually have to change by exactly the same amount at *all* points around its circumference, even though the reduction in wall thickness occurs at only one point. So, how do curvature changes occur in ring rolling?

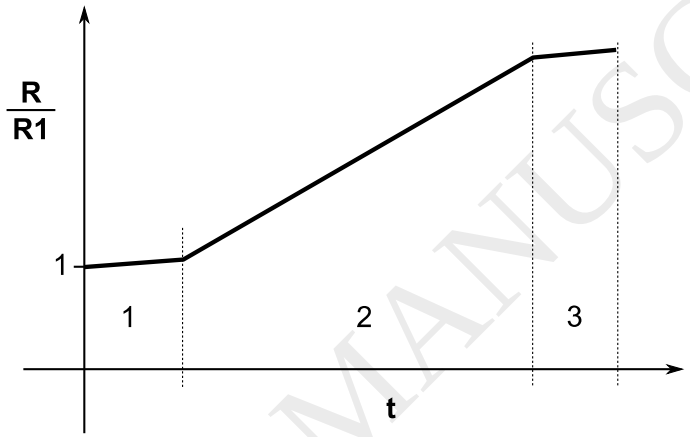

Fig 3 Average radius of curvature against time in an illustrative ring rolling process.

As far as the authors are aware none of the analytical models of ring rolling in the literature are able to predict changes in curvature. Briefly reviewing such models, Hawkyard et al. (1973) predicted roll forces and torque by analogy to plane strain indentation by opposed flat indenters, determining correction factors for the average roll pressure. They justified this choice of this model – over classical slab modelling – on the grounds that the ratio of wall thickness to contact length is usually much greater than unity. The effect on roll force of unequal reductions and incoming ring curvature were both considered; however the mechanism by which curvature develops was not explored.

Parvisi et al. (2011) used a modified slab model to predict the roll force and torque in ring rolling. They show the torque prediction is accurate to within approximately 20%, but do not provide experimental validation of the roll force or pressure profile along the contact length. Changes in ring curvature are not explicitly considered.

Johnson and Needham (1968), investigated the possibility of a plastic hinge occurring *outside* of the radial roll gap region, as the material in the radial roll gap lengthens circumferentially. They statically indented a ring workpiece at the top of ring, as shown in Fig 4, gradually increased the indentation load and found that once the thickness strain reached approximately -0.18, a plastic hinge was observable opposite the point of indentation. This was a single indentation at one point around the ring; in the continuous process plastic curvature changes could potentially occur by the cumulative effect of smaller wall thickness reductions.

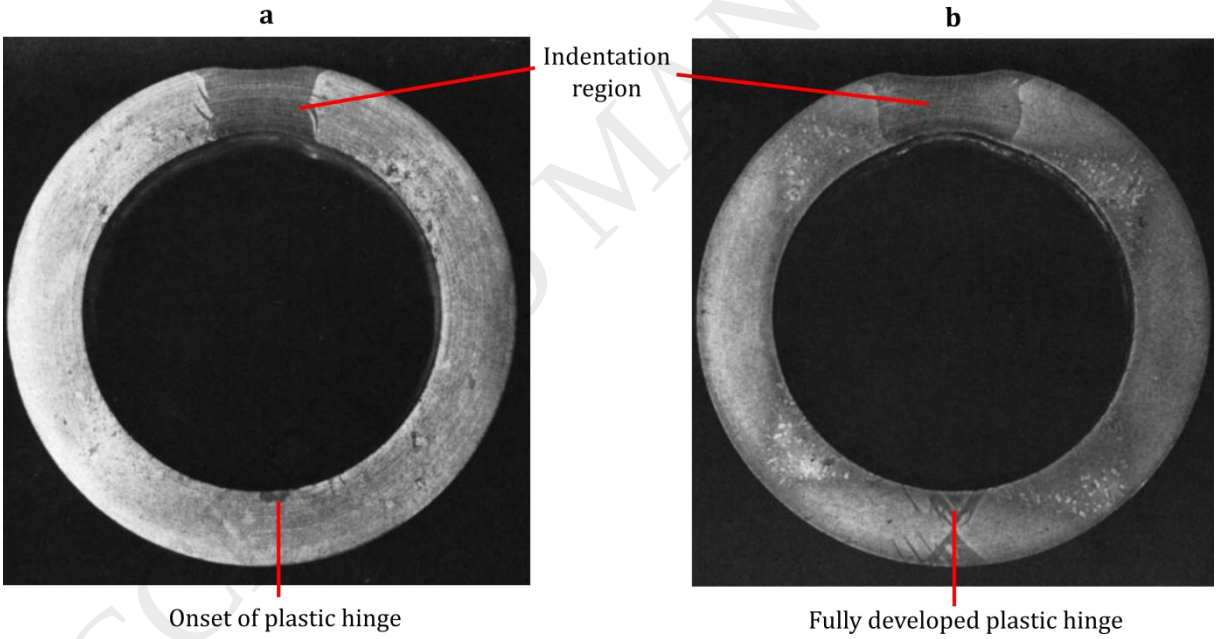

Fig 4 Plastic hinge formation in static ring indentation **a.** onset of hinge **b.** fully formed hinge (Johnson and Needham, 1968). Images reproduced with permission of Elsevier

Whilst this is a possible source of plastic curvature change in ring rolling, it is also likely that there are changes in curvature across the radial forming zone itself. Several studies into flat strip rolling have investigated this.

Johnson and Needham (1966) showed experimentally that asymmetries in the roll diameter, surface speed and surface roughness in flat strip rolling can each result in curvature changes. The interaction of these factors was demonstrated; whereas unequal roll speeds might ordinarily result in curvature towards the slowest roll, this can be cancelled out if this roll is also smoother. The reduction in thickness was found to play a role in 'amplifying' the changes due each of the factors; particularly unequal roll diameters.

Collins and Dewhurst (1975) used a slipline field analysis to predict the curvature change in asymmetric rolling. In their study the slab was constrained by a rolling table at the entry side so that the reduction at each roll is equal. The analysis that predicts – for a given reduction in thickness - a reversal in curvature as the roll-size ratio changes, a phenomenon also observed experimentally (see Fig 5). The reason for this oscillation is not clear.

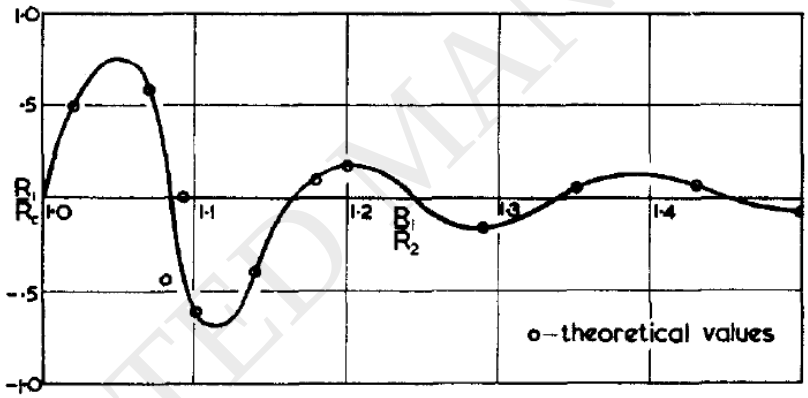

Fig 5 Variation of outgoing strip curvature (Rc) in asymmetric rolling with changing ratio of roll radii, (R1, R2). For *R1/T* = 10, thickness reduction 20% (Collins and Dewhurst, 1975) Image reproduced with permission of Elsevier

Shivpuri et al. (1988) used finite element analysis to predict the effect of variable roll speed on curvature change during flat strip rolling. With equal diameter rolls and friction, and free entry conditions, speed mismatches in the order of 0-10% were considered. Their analysis predicted curling of the strip towards the slowest roll, largely in line experimentally obtained

values. They attribute the difference to self-weight of the strip inducing a moment at the roll entry, an effect they did not model.

Salimi and Sassani (2002) provide a modified slab model to predict changes in strip curvature in asymmetric rolling. The model accounts for curvature changes due to differences both in the shear and axial strains through the height of the strip. The effect of differential roll surface speed and friction factors are predicted and compared to experimental results; both are shown to play a significant role. The effect of roll radius on curvature is not explicitly explored.

Minton and Brambley (2017) reviewed eight such experimental studies and nine numerical studies. Their regression analysis tentatively indicates three main trends: curvature away from the fastest roll, towards the roughest roll and away from the largest roll. They do not claim predictive power, but instead use the analysis to highlight the complexity of the problem and the limitations of current analytical models (offering the Salimi and Sassani model as a case study) to predict curvature changes over the full range of possible asymmetries in flat strip rolling.

None of these studies considered curvature change on open-ended strips in conditions reflecting the ring rolling process. These are markedly different from asymmetric strip rolling. The internal roll is not powered and so will not 'drive' any difference in curvature. The rolls' axes are typically vertical and so gravity and the support table will have little influence. The workpiece is initially curved. The roll diameters, especially the mandrel, are comparably smaller, as is the reduction in thickness per pass, and so the contact length is typically much smaller compared to the workpiece thickness. Because of these factors this paper chooses to develop a new – and rather simpler – approach to predicting open-ended curvature change as a step to understanding how curvature changes are regulated in ring rolling.

This paper assumes that curvature change in such conditions are principally influenced by differences in the reduction in thickness at each roll. The work of Hawkyard et al. (1973) provides a prediction of this reduction share for closed rings – the ratio of the thickness

reduction at the forming roll (ΔT_F) to the mandrel (ΔT_M). Building on their slip-line theory model for roll force and using geometrical arguments they propose that in ring rolling:

$$\Delta T_F/\Delta T_M \cong \left(\frac{IR/R_F+1}{IR/R_M+1}\right)^{1/2}\left(\frac{\bar{R}}{OR}\right)^{-1} \quad [2]$$

where *IR* and *OR* are the inner and outer ring radii, $\bar{R} = (\mathrm{IR} + \mathrm{OR})/2$ is the mean ring radius, and R_F and R_M are the forming roll and mandrel radii.

Using the form of Equation 2, Koppers and Kopp (1992) provided Equation 3, an empirical prediction of the reduction share when R_F and R_M were 377mm and 62.5mm respectively:

$$\Delta T_F/\Delta T_M = 3.36\left(R_{Mf}/R_{Ff}\right)^{1.46}(\bar{R}/OR)^{5.23} \quad [3]$$

Equation 3 contains the effective tool radii, R_{Mf} and R_{Ff} proposed by Koppers and Kopp as measures of tool size that take into account the fact that the curvature of the workpiece makes the inner tool 'appear' larger than it is and the outer tool smaller. These are defined in Equations 4 and 5 respectively.

$$R_{Mf} = \frac{R_M IR}{IR-R_M} \quad [4]$$

$$R_{Ff} = \frac{R_F OR}{OR+R_F} \quad [5]$$

They argued that provided $IR/R_M>1.5$, the following relationship between contact length, L, reduction in thickness, ΔT, and roll radius R_{if}, is valid: $L \cong \sqrt[2]{2\Delta T R_{if}}$.

In ring rolling it is known that the guide rolls play a role in regulating curvature change. Hua et. al. (2016) recommend that to maintain stability the guide rolls should not induce bending stresses in the ring that exceed yield. They propose that if the guide rolls are to be force-controlled, the force should be adjusted throughout the process to be constant factor (k_g from 0-1) of this maximum guide roll force. This factor appears to be empirically determined.

Stress-superposition theory might provide an explanation for how the guide rolls are effective despite applying forces below those which could cause a permanent curvature change in isolation. Becker et al. (2014) amongst others have shown that relatively small applied moments can create permanent curvature change if a workpiece is simultaneously undergoing plastic deformation through a separate process. In the incremental tube forming process they studied, a tube is simultaneously bent whilst undergoing a diameter reduction by spinning. The bending moment was experimentally found to reduce to $1/20^{th}$ of its value for a 5% diameter reduction. This type of analysis has not yet been explicitly extended to ring rolling.

1.2 Structure of this paper

This paper firstly investigates curvature change in the radial roll gap alone decoupled from the influence of the rest of the ring (Section 2), through both experiments and numerical simulations. This is a ring rolling equivalent to the Johnson and Needham (1966) and subsequent studies on asymmetric flat strip rolling. In this it will be necessary to develop new predictions for the share in the reduction in thickness at each roll.

Then, in Section 3 the effect of rolling a full ring is considered through numerical simulation. First an elastic moment is applied to the workpiece; and a relationship between the moment and the curvature change is established and presented in Section 3a, along the lines of Becker et al. (2014). Finally, in Section 3b the rolling of a full ring is considered. Here, the knowledge in Sections 2 and 3a are combined to predict the value of the internal bending moment at the roll-gap, as well as observing the extent to which curvature changes occur outside of the rollgap region – such as those reported by Johnson and Needham (1968) in static indentation.

2 Curvature changes in free-ended half rings

To help build a complete picture of curvature change in ring rolling, firstly the curvature changes in the radial roll bite in isolation are considered. A free-ended half ring is considered so that the 'free curvature change' can be understood; i.e. the curvature change that would occur in isolation from the elastic boundary conditions that the rest of the ring imposes. It is of great interest to know if the free curvature change matches the changes in curvature found during (full) ring rolling. If not, then some mechanism of correction is required in the full process, and the ring is likely to be subject to internal stress.

To investigate the free curvature change, the set-up shown in Fig 6 was used. The workpiece is initially a half ring ($\phi_{Tot}1$=180°) of known initial wall thickness, $T1$, and average radius, $\bar{R}1$. It is indented by nominal reduction in thickness ΔT at an angle 15° around the circumference, by translating the mandrel in the x-direction with the forming roll held stationary. The forming roll is then set to rotate at constant angular speed, drawing the ring through the fixed roll gap, and stopping so that an angle $\phi 1 = 150°$ of the original arc is rolled. No guide rolls act on the ring

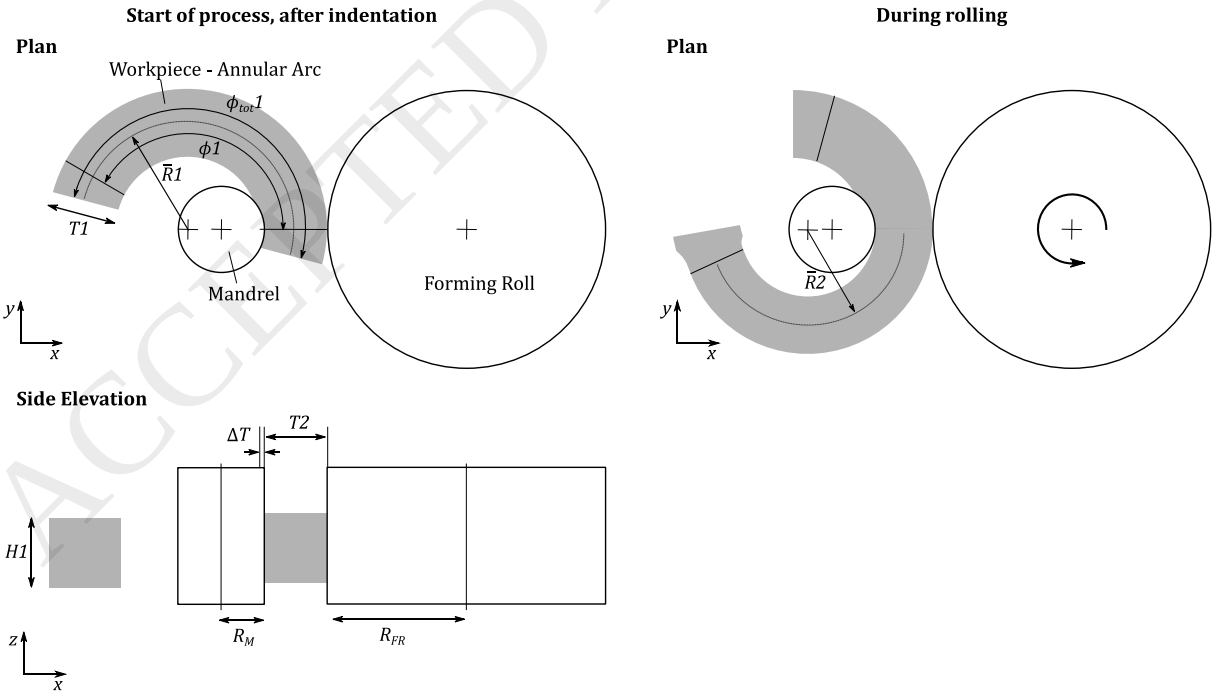

Fig 6 Schematic set-up for experiments and simulations on free curvature change of half rings

The primary interest is the change in the radius of curvature across the radial roll bite. The non-dimensional parameter χ_{free} as defined below, is used:

$$\chi_{free} = \frac{\bar{R}2}{\bar{R}1} \quad [6]$$

where $\bar{R}2$ is the mean outgoing radius. In the proceeding investigation the effect of two key variables thought to influence curvature change will be investigated; the % nominal reduction, δ, Eqn 7, and the effective tool size ratio, ζ, Eqn 8.

$$\delta = \frac{\Delta T}{T1} = \frac{T1-T2}{T1} \quad [7]$$

$$\zeta = \frac{R_{Mf}}{R_{Ff}} \quad [8]$$

where R_{Mf} and R_{Ff} are the effective tool radii as defined in Eqns 4 and 5 above.

The tool size ratio is thought to affect the degree to which deformation is localised on either the outer or inner surface and hence generate positive or negative curvature change respectively.

Asymmetry in frictional conditions is beyond the scope of the present study. Although the literature has shown frictional asymmetry does have an influence in strip rolling this may not be such a significant factor in open-ended ring rolling, since only the forming roll is powered and the contact length is relatively short.

In addition to the reduction and tool size ratio, Table 1 summarises the other key variables in this study. Two different starting ring geometries were considered representing a 'thick' and 'medium' walled ring as a way to test the validity of the model. The thickness strain rate is the average in the roll bite calculated a-priori. Its value was held constant by adjusting the rotation speed of the forming roll accordingly.

Table 1 Summary of variables used in this study

Quantity	Description	Value(s) used in this study
δ	Reduction in wall thickness	0.02 – 0.10
ζ	Effective tool size ratio	0.75, 1.0, 1.33, 2.1
$\overline{R1}/_{T1}$	Ring slenderness	188 mm /30 mm = 6.26 and 106 mm / 50 mm = 2.12
$\dot{\bar{\varepsilon}}$	Thickness strain rate	0.2 / s
$H1/_{T1}$	Blank aspect ratio	30 mm / 30 mm = 1.0 and 34 mm / 50 mm = 0.68
$R_{FR}/_{T1}$	Forming roll radius to wall thickness ratio	100 mm / 30 mm = 3.33 and 100 mm / 50 mm = 2.00

The free curvature change was investigated through Finite Element Modelling (FEM), experiments and predicted by an analytical model. The analytical model is described next, followed by the experimental and simulation methods before finally summarising the overall 'Design of Experiments'.

2.1 Analytical prediction of 'free' curvature change

An analytical model is proposed to explain and predict the free curvature change. An accurate analytical prediction of the 'free' curvature change could inform tool design and process layout for better circularity/reduced internal stress.

The model is summarised in Fig 7. It computes the final radius of curvature that would generate an assumed thickness strain distribution that is in turn compatible with a prediction for the thickness reduction at each roll.

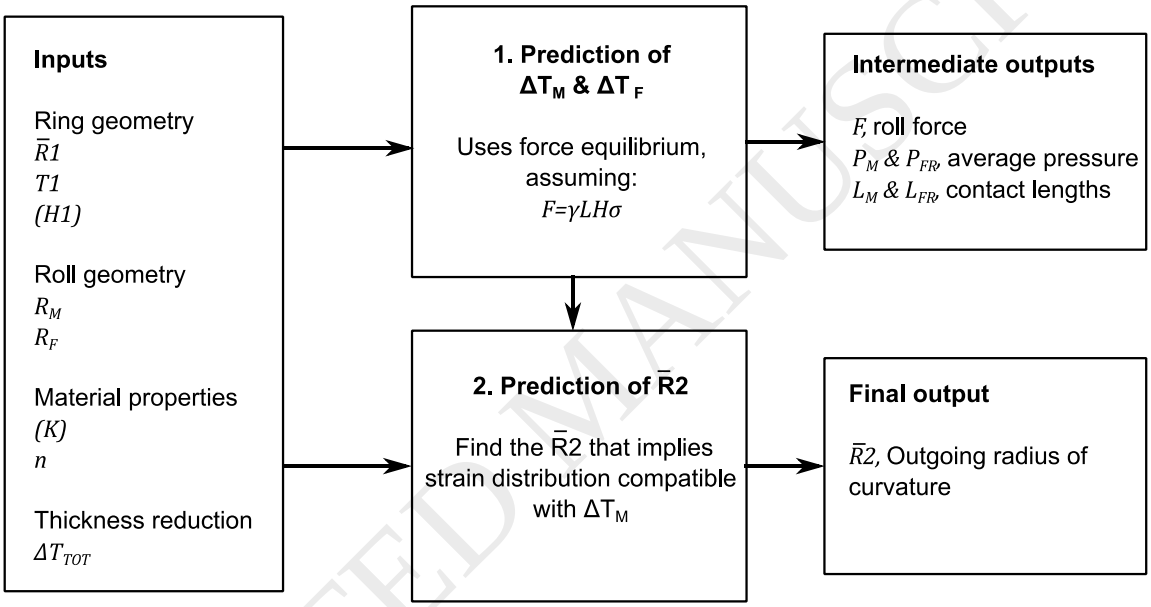

Fig 7 Overview of the model of this paper for free curvature change in ring rolling

Examining the contact conditions in ring rolling, it is apparent that the thickness reduction at each roll ΔT_M and ΔT_F for the mandrel and forming roll are potentially unequal (Fig 8a). This will have a profound consequence for the outgoing curvature if the workpiece is not otherwise constrained. This principal is illustrated in Fig 8 b and c: if ΔT_M is larger than ΔT_F – for instance because the mandrel's effective radius is much smaller than the forming roll, the consequential circumferential extension would concentrate nearest the mandrel and the ring curve 'away' from it. Or vice versa.

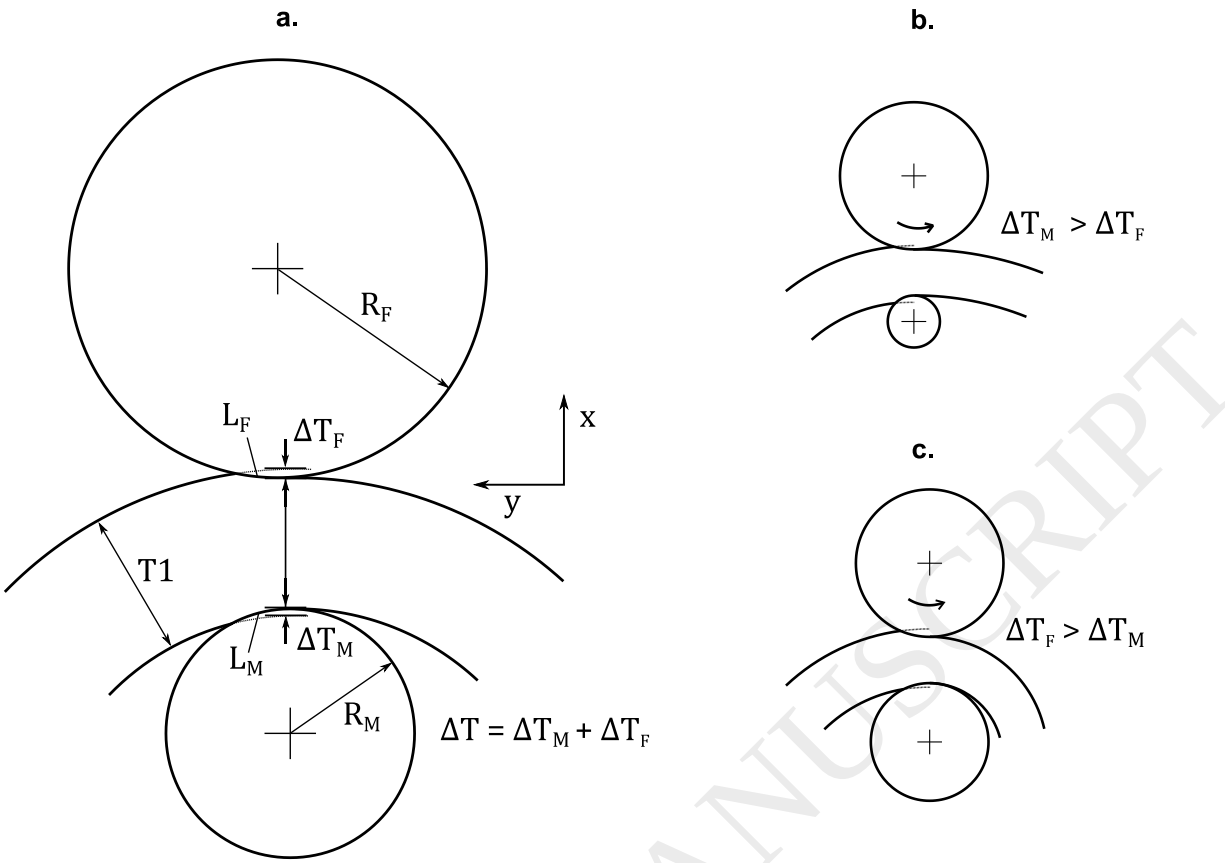

Fig 8 a. Contact geometry schematic **b.** & **c.** illustration of the effect of tool size on free curvature change

To predict the different reductions in thickness, ΔT_M and ΔT_F, a simple estimate for how the roll force relates to the reduction is made at each roll and then equilibrium is invoked for which a unique solution for ΔT_M and ΔT_F is found. This approach will be compared to results obtained by using the direct predictions (Equations 2 & 3 above) applicable to rolling of complete rings.

These thickness reductions are subject to the constraint that – neglecting elasticity:

$$\Delta T_M + \Delta T_F = T1 - T2 \qquad [9]$$

The projected contact length in the y direction at each roll is:

$$L_i = \sqrt[2]{2\Delta T_i R_{if} - {\Delta T_i}^2} \qquad [10]$$

The roll pressure is neither constant along each contact length, nor does it have the same average value. A well-established model for the average pressure factor, γ_i during ring rolling (in which the ratio of contact length to wall thickness is small - markedly different to flat rolling where slab theory is commonly used) is the slip-line field solution for plane strain indentation by opposed flat indenters, as described by Hawkyard et al., 1973. This paper assumes that the analysis can be applied separately to each 'half' of the ring of wall thickness T/2. In this case, the roll force, F_i, on either mandrel F_M or forming roll F_F is given by:

$$F_i = 2k_i\gamma_i L_i H \qquad [11]$$

where k_i is the yield shear stress in plane strain and H is the ring's axial height.

The slipline solution for the pressure factor is shown in Fig 9:

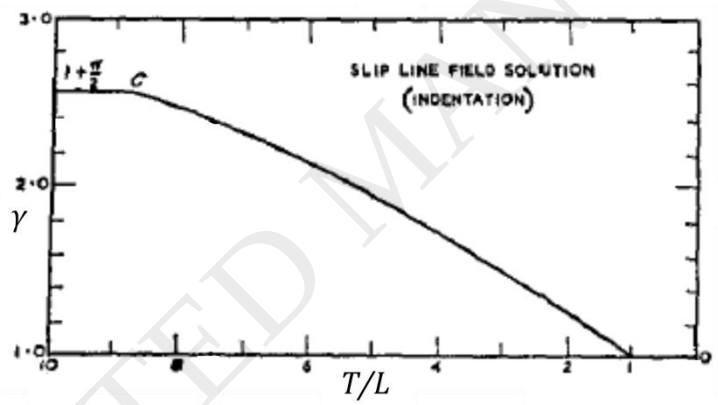

Fig 9 Variation of the pressure factor, γ with $\frac{L_i}{T}$ (Hawkyard et al. 1973). Image reproduced with permission from Elsevier.

The following function for the variation of factor, γ_i, with $\frac{L_i}{T}$ is used to approximate the relationship graphed in Fig 9:

$$\gamma_i = \begin{cases} 1+\frac{\pi}{2}, & \frac{L_i}{T} > 8.74 \\ 0.203\frac{L_i}{T} + 0.797, & 1 < \frac{L_i}{T} < 8.74 \\ 1, & \frac{L_i}{T} < 1 \end{cases} \qquad [12]$$

where T is the average wall thickness.

Following the Hawkyard et al. 1973 approach, hardening can be accounted for by assuming that the equivalent strain is:

$$\bar{\varepsilon}_i = \frac{2}{\sqrt{3}}\gamma_i \ln\left(1 - \frac{2\Delta T_i}{T1}\right) \quad [13]$$

The yield shear stress in plane strain at each roll is:

$$2k_i = \frac{2}{\sqrt{3}} K \bar{\varepsilon}_i^{\,n} \quad [14]$$

Combining Eqns 11, 12, 13 & 14 the force at each roll is (for $1 < \frac{L_i}{T} < 8.74$) :

$$F_i = \frac{2}{\sqrt{3}} K \left[\frac{2}{\sqrt{3}}\gamma_i \ln\left(1 - \frac{2\Delta T_i}{T1}\right)\right]^n \left(\frac{0.203\sqrt{2\Delta T_i R_{ieff} - \Delta T_i{}^2}}{T} + 0.797\right)\left(\sqrt{2\Delta T_i R_{ieff} - \Delta T_i{}^2}\right) H \quad [15]$$

Using Eqns 15 & 9, F_M and F_{FR} can be made to be functions of a single unknown variable – say ΔT_M. For equilibrium in the y direction these must be equal, and so ΔT_M is found by solving the equation:

$$F_M(\Delta T_M) = F_F(\Delta T_M) \quad [16]$$

A closed form solution is not tractable. However, for reasonable values of the quantities involved F_M and F_F are respectively monotonically increasing and decreasing functions of ΔT_M and so a solution for ΔT_M can be found by interpolation of the function $F_M - F_F$ evaluated at grid of values for ΔT_M in the range 0 to T2.

The second component of the analytical model (Fig 7) relate the reductions ΔT_M and ΔT_{FR} to the outgoing radius of curvature. To do this it is assumed that the outgoing rolled material in the centre of the ring remains an arc as sketched in Fig 10, and then a strain field compatible with the reductions is computed.

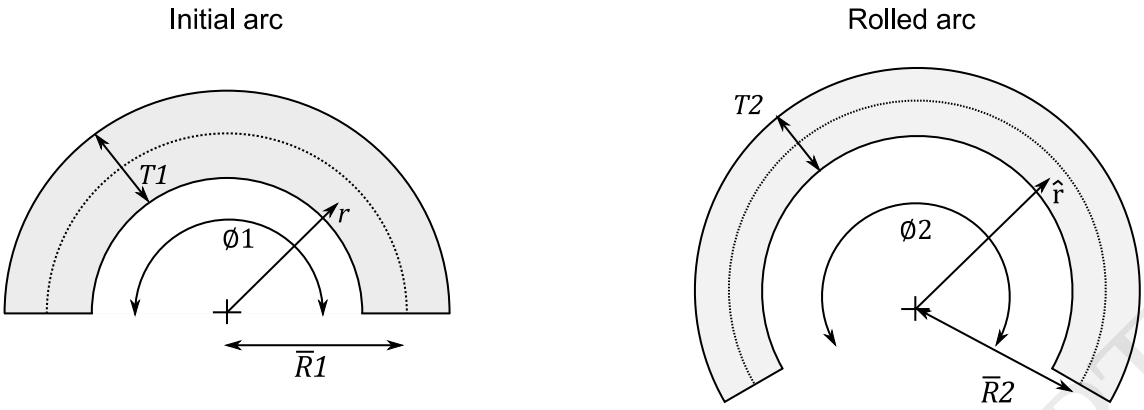

Fig 10 Assumed geometry of the rolled arc

The strain in the circumferential direction as a function of initial radial location, r, and the corresponding final radial position, $\hat{r}$ is :

$$\varepsilon_c(r) = \ln\left(\frac{\phi 2\hat{r}}{\phi 1 r}\right) \quad [17]$$

By applying volume constancy and assuming no height growth it is found that:

$$\frac{\emptyset_1}{\emptyset_2} = \frac{(\bar{R}_2 T_2)}{(\bar{R}_1 T_1)} \quad [18]$$

$$\hat{r} = \sqrt{\left[\frac{\emptyset_1}{\emptyset_2}\left(r^2 - {IR_1}^2\right) + {IR_2}^2\right]} \quad [19]$$

Combining Eqns 17, 18 & 19, together with the plane strain assumption gives the thickness strain:

$$\varepsilon_t(r) = -\varepsilon_c(r) = -\ln\left(\frac{\emptyset_2\sqrt{\left[\frac{\emptyset_1}{\emptyset_2}\left(r^2 - {IR_1}^2\right) + {IR_2}^2\right]}}{\emptyset_1 r}\right) \quad [20]$$

And so the reduction in thickness at the mandrel, $\Delta\widehat{T_M}$, based on the outgoing radius, is:

$$\Delta\widehat{T_M} = \int_{IR_1}^{\bar{R}_1} \varepsilon_t(r)\, dr \quad [21]$$

$$\Delta\widehat{T_M} = \int_{IR_1}^{\bar{R}_1} -\ln\left(\frac{\sqrt{\left[\frac{(\bar{R}_2 T_2)}{(\bar{R}_1 T_1)}\left(r^2 - {IR_1}^2\right) + {IR_2}^2\right]}}{\frac{(\bar{R}_2 T_2)}{(\bar{R}_1 T_1)} r}\right) dr \quad [22]$$

The outgoing radius, $\bar{R}2$ is found by setting $\Delta\widehat{T_M}$ equal to the reduction in thickness found by solving Equation 16 above. Again, since $\Delta\widehat{T_M}$ is a monotonically increasing function of the outgoing radius $\bar{R}2$, the solution – and hence predicted value of the free curvature change can be found by interpolation.

Figure 11 illustrates the predicted value for the free curvature change, $\chi_{free} = {\bar{R}2}/{\bar{R}1}$ as a function of the reduction in thickness and the effective tool size ratio. As was illustrated in Fig 8 this predicts a strong dependency on the tool size ratio. As the mandrel becomes larger the radius of curvature is predicted to *decrease* significantly. It is interesting to note that with an effective tool size ratio of unity the ring is predicted to 'curl up'. In this case equal thickness reductions at each roll are expected and so the inner and outer surface arcs would extend by the same *proportion*. However since the outer surface arc is *initially longer* the compatible product has a smaller average radius.

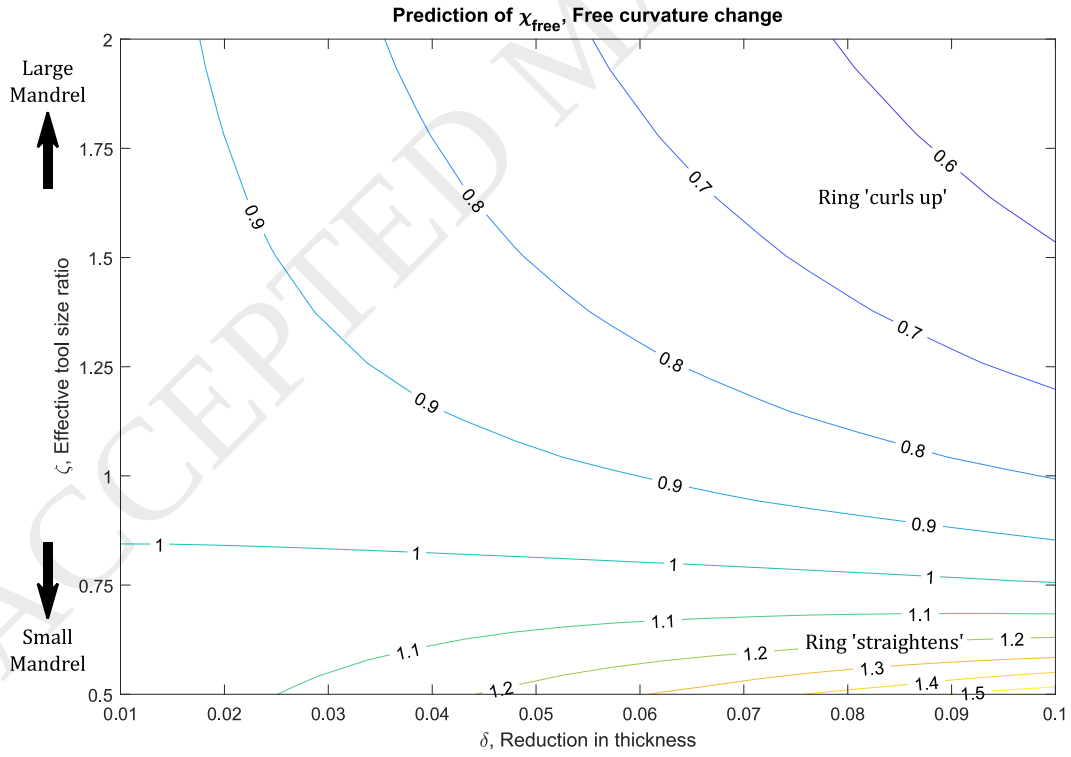

Fig 11 Prediction of the free curvature change in ring rolling, varying tool size ratio and reduction. Ring slenderness $\bar{R}/T$ = 6.3, strain hardening coefficient, n=0.17

To test this new analytical model for the free curvature change a set of experiments and finite element simulations were carried out. These are now described.

2.2 Methodology: experiments

A set of twenty experiments were carried out using the set up described in Fig. 6, on the University of Cambridge Constrained Incremental Ring Rolling machine (Cleaver and Allwood, 2017). Fig 12 shows the workpiece resting on table rolls being rolled between the powered outer forming roll and inner mandrel.

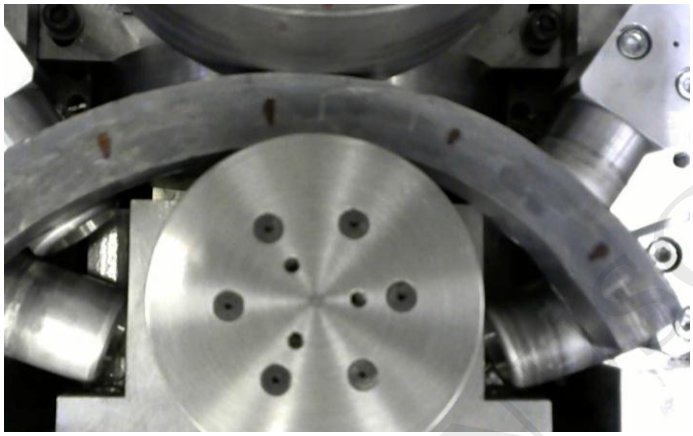

Fig 12 Workpiece in machine during free curvature experiment

Prior to the free curvature experiments the preform was created by pre-rolling a cast blank to a uniform thickness and specified outer radius (203mm or 132mm). Due to inconsistencies in the volume of the initial cast blank, the initial workpiece thickness varied slightly from the nominal values given in Table 1 above. The thickness setpoints in the free curvature experiments were adjusted so that the percentage thickness reductions were exactly as required. A small overclosure was added to compensate for the compliance of the machine, using force data from a load cell on the radial roll gap and known machine stiffness. Measurements at seven points around the half ring with a micrometer confirmed that the targeted thickness change was achieved.

The workpiece material is 99.8% pure Lead BS EN 12588, chosen as a representative model material that is deformable at room temperature within the force capacity of the experimental equipment. In order to carry out numerical and analytical modelling, flow curves

were determined through uniaxial compression tests on cylindrical specimens cut from the pre-rolled ring, aligned with the thickness direction.

The compression test specimens were of initial diameter 20mm and height 20mm. Tests were carried out at five true strain rates: 0.01/s, 0.1/s, 0.2/s 0.4/s and 1/s. Lubrication was provided by inserting a 0.05mm thick PTFE sheet between the sample and the upper and lower platen respectively. The sheets were discarded and replaced after each test. Other studies have shown this can reduce the coefficient of friction to μ= 0.01 (Christiansen, Martins & Bay, 2016).

The flow curves are shown in Fig 13. The flow stress rises initially before levelling off when the strain reaches values in the range 0.2 to 0.5. In all except the 1/s the material clearly softens after the reaching these peak values: in the 0.01/s case the flow stress reduces by 6.8 %. The recrystallization temperature for pure lead is -80°C (Schmidt & Haessner, 1991), and so it is likely that this softening is due to dynamic recrystallization. It may only show up on the flow curve at slower strain rates because of the diffusional kinetics. The peak stress (21.9, 26.0, 28.0, 29.6, 31.5) value increases with increasing strain rate. This moderate visco-plasticity is characteristic of materials in a high temperature regime relative to its melting point.

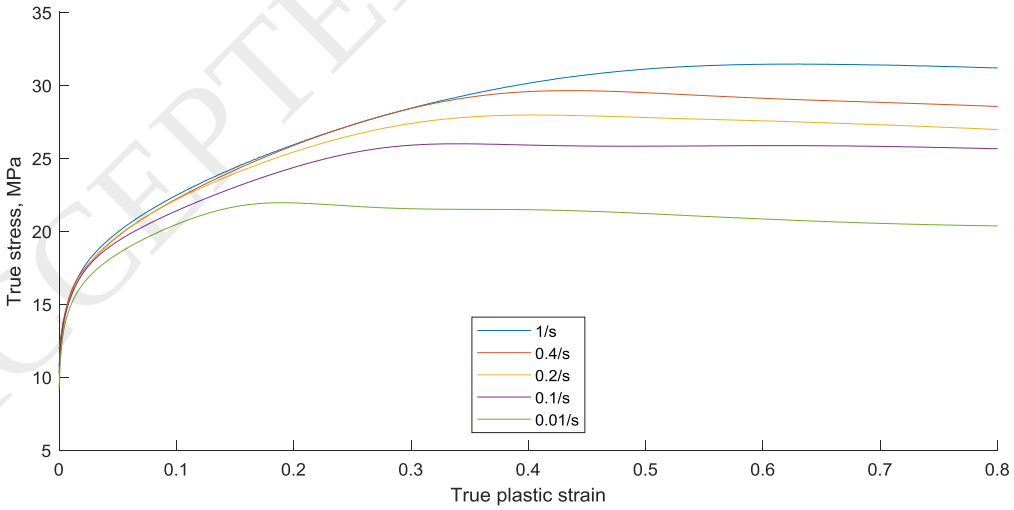

Fig 13 Flow curves for 99.8% pure Lead used in experiments in uniaxial compression tests

The free curvature experiments were undertaken at an average strain rate 0.2/s, for thickness strain up to a value of 0.127. For the purpose of the analytical model a fit to the data in the form $\bar{\sigma} = K\varepsilon^n$ was obtained on the 0.2/s data in the range ε = 0.01 - 0.2. The resulting values of K and n are tabulated in Table 2 below.

Table 2 Flow curve fit to the model $\bar{\sigma} = K\varepsilon^n$ for $\dot{\varepsilon}$ = 0.2/s in region ε = 0-0.2

Parameter	**Value**
K	33.1
n	0.17

The radius of curvature before and after rolling was measured by first creating an outline of the shape taking 38 measurements around the ring using a Mitutoyo CMM machine (Fig 14a). An interpolated surface was created between these points and then the average radius of curvature of the outer surface and inner surface were determined from three points around this surface spanning the central 120° of the workpiece as indicated in Fig 14b.

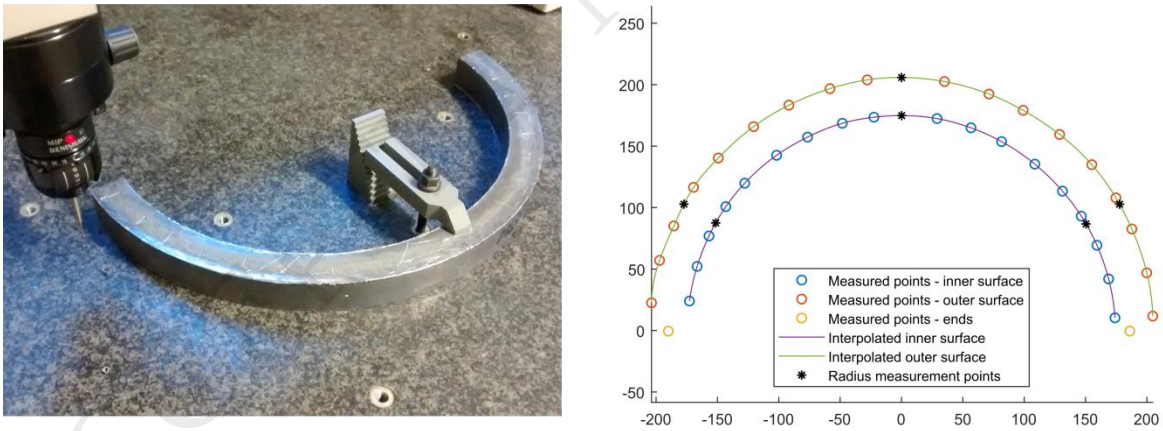

Fig 14 a. CMM machine **b.** Example shape outline and radius measurement points

2.3 Methodology: FEM

Finite element method (FEM) simulations were carried out to provide extra resolution in the test points and interrogate features not easily measured experimentally such as the roll pressure distribution and the loci of contact. Later, FEM is also used to predict the effect of an end-moment on the arc, and the internal stress state during rolling of a full ring.

The simulations were carried out in the commercial package ABAQUS/Standard, release v16.45. The implicit solver was selected over the explicit solver since an accurate prediction of residual stress was believed to be important to the investigations in Section 3. The simulation was made in 3-D, using linear reduced integration elements. To reduce the size of the problem and increase stability, symmetrical behaviour in the axial direction was assumed and only half of the workpiece was modelled.

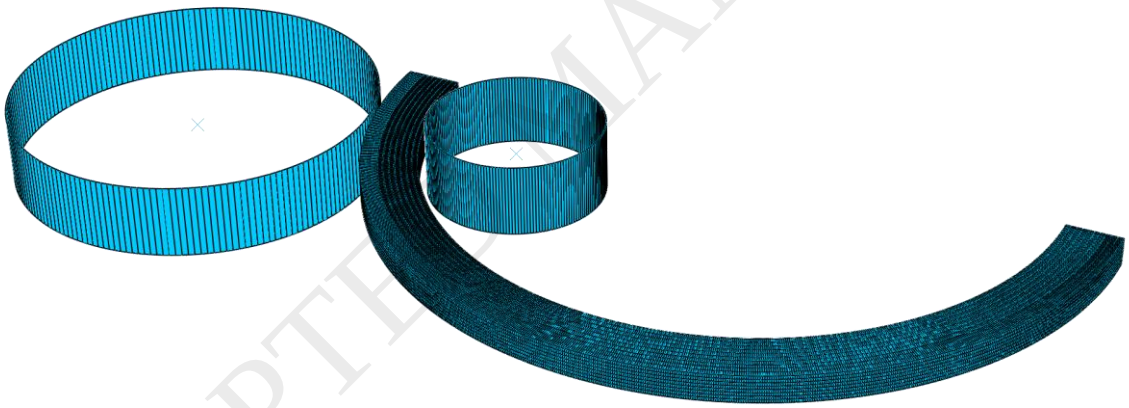

Fig 15 FEM model assembly set-up

The main parameters used in the simulation were as listed in Table 3. The mesh was chosen with care to ensure that between 5-14 elements around the circumference would occupy the predicted length of contact (from 6mm to 15mm for low and high reductions respectively); the chosen value was believed to be an appropriate trade-off between accuracy and solution time and is comparable to previous studies.

Two features were used to ensure that the solution would converge. Contact stabilization was used, introducing artificial contact damping to surfaces with clearance from 0 to 0.05mm (i.e. the roll entry and roll exit). The maximum value of this stress was in the region of 0.8 MPa, 1.3% of the peak contact stress. Exponential contact was used to smoothly model the normal pressure to clearance relationship; so that the pressure sharply rises from 0 MPa at 0.02mm clearance to 500MPa at 0.00mm clearance. The actual contact pressure ranged from 40-60 MPa, suggesting the rollgap as modelled could be up to 0.02mm smaller than it really is: equivalent to a 0.07% additional reduction in thickness.

Table 3 Parameters used in the Finite Element Simulation

Feature	**Details**
Contact	Exponential contact: • 500MPa @ 0.00mm clearance • 0 MPa @ 0.02 mm clearance Coulomb friction, μ = 0.3 Contact stabilization: • Stabilization factor: 0.01 • Clearance at which stabilization is zero: 0.05mm • Factor at end of rolling phase: 0
Material Model	Young's modulus: 50MPa Tabulated plastic flow curve at strain rates: • 0, 0.01/s, 0.1/s, 0.2/s, 1/s • as per Fig 13
Workpiece	Element type: C3D8R (8 node brick with reduced integration) Mesh size: 600 circumferential x 10 radial x 8 axial = 48,000 elements
Tools	Analytical rigid bodies

A sensitivity study on the value of the friction coefficient was carried out. In this, the mandrel to forming roll effective size ratio was set at 1.0 and 1.33, the nominal reduction in thickness was 8% and the friction coefficient was varied from μ = {0.2, 0.25, 0.30, 0.35, 0.40}. The outgoing curvature is relatively insensitive to the friction coefficient in the range μ =0.2 –

0.4, varying by just 2% for both tool size ratios – see Table 4. For values somewhat smaller than 0.2 – for this reduction – the workpiece is no longer drawn into the rollgap. This is as expected from the 'biting-in' condition. The value 0.3 was chosen with some confidence that this would only weakly influence the result. The insensitivity to friction coefficient even when the tool sizes are not equal suggest that the 'friction hill' effect is not a significant factor in the conditions studied, supporting the choice to use a plane strain indentation model.

Table 4 Sensitivity of the free curvature change, χ_{free}, to the friction coefficient, μ. FEM simulation with tool size ratio, ζ=1.0 and 1.33, and reduction, δ=0.08

Friction coefficient	ζ=1.0	ζ=1.33
	$\boldsymbol{\chi_{free}}$	$\boldsymbol{\chi_{free}}$
0.2	0.91	0.79
0.25	0.90	0.78
0.3	0.89	0.77
0.35	0.89	0.78
0.40	0.89	0.78

2.4 Design of Experiments & FEM

A summary of the experiments and numerical simulations on free curvature change is given in Table 5. For the medium-walled ring, twelve experiments were carried out spanning three different tool size ratios (ζ) and four different reductions in thickness (δ). A further eight experiments were carried out on thicker-walled rings. The study therefore covers a significant proportion of the range of conditions usually encountered in industrial practice in ring rolling. In each experiment the forming roll speed was varied to ensure that the average thickness strain rate was 0.2/s. The numerical simulations cover a slightly larger range of eight reductions in thickness.

Table 5 'Design of experiments' for free curvature change experiments and FEM

Ring sizing	Tool size ratio, ζ	Reduction in thickness, δ	
		Experiments	FEM
IR = 173 mm OR = 203 mm H = 30 mm	0.75 (R_M = 39.0 mm, R_F = 100 mm)	0.04, 0.06, 0.08 & 0.10	0.01, 0.02, 0.03, 0.04, 0.05, 0.06, 0.08 & 0.10
	1.00 (R_M = 48.3 mm, R_F = 100 mm)	0.04, 0.06, 0.08 & 0.10	0.01, 0.02, 0.03, 0.04, 0.05, 0.06, 0.08 & 0.10
	1.33 (R_M = 58.9 mm , R_F = 100 mm)	0.04, 0.06, 0.08 & 0.10	0.01, 0.02, 0.03, 0.04, 0.05, 0.06, 0.08 & 0.10
IR = 81 mm OR = 131 mm H = 34 mm	1.33 (R_M = 39.0 mm , R_F = 100 mm)	0.04, 0.06, 0.08 & 0.10	
	2.12 (R_M = 48.3 mm, R_F = 100 mm)	0.04, 0.06, 0.08 & 0.10	

2.5 Results and analysis

The experimental results, finite element simulations and analytical predictions for free curvature change are now presented. The experimental results are shown in Fig 16 for varying tool size ratio, ζ (up and down) and reduction, δ (left to right). Whereas during the conventional ring rolling process the radius of curvature increases, it is very clear that when a free-ended half ring is rolled the opposite is possible: the radius can decrease and the ring 'curls up'.

As predicted by the analytical model, the effective tool size ratio $\zeta = R_{Mf}/R_{Ff}$ has a significant effect on the outgoing free curvature, $\chi_{free} = \bar{R}2/\bar{R}1$. As ζ increases and the inner tool gets larger, χ_{free} decreases. This is most obvious at the largest reductions, where for ζ = 0.75, χ_{free} is 1.01, but when ζ = 1.33, χ_{free} has reduced to 0.61.

The reduction in thickness, δ, 'amplifies' the changes in curvature. For example, with ζ =1.33, a value of δ of 4% results in χ_{free} of 0.87, whereas values of δ of 6, 8 and 10% give $\chi_{free}$of 0.82, 0.72 and 0.61 respectively.

The same trend is seen in the thick-walled rings, as shown in Fig 17. For the same tool size ratio (ζ =1.33) the amount of curvature change is not as large in the medium-walled case. For example, with δ = 10%, χ_{free} is 0.84, whereas it was 0.61 for the medium-wall ring. Interestingly a further increase in the tool size ratio, ζ, to a value of 2.1 only results in a small increase in the curvature change.

The FEM and experimental results for the medium walled rings are compared back-to-back in Fig 18. There is significant agreement with the trends described above. The results for tool size ratio ζ = 0.75 are most obviously in agreement, whereas there is some divergence on the other tool size ratios for larger reductions in thickness.

Fig 16 Experimental results for free curvature change in ring rolling of half rings for various tool size ratios (ζ) and reductions in thickness (δ)

Fig 17 Comparison of free curvature change for medium-walled and thick-walled half rings, with tool size ratio ζ = 1.33 and 2.12, varying the reduction in thickness (δ)

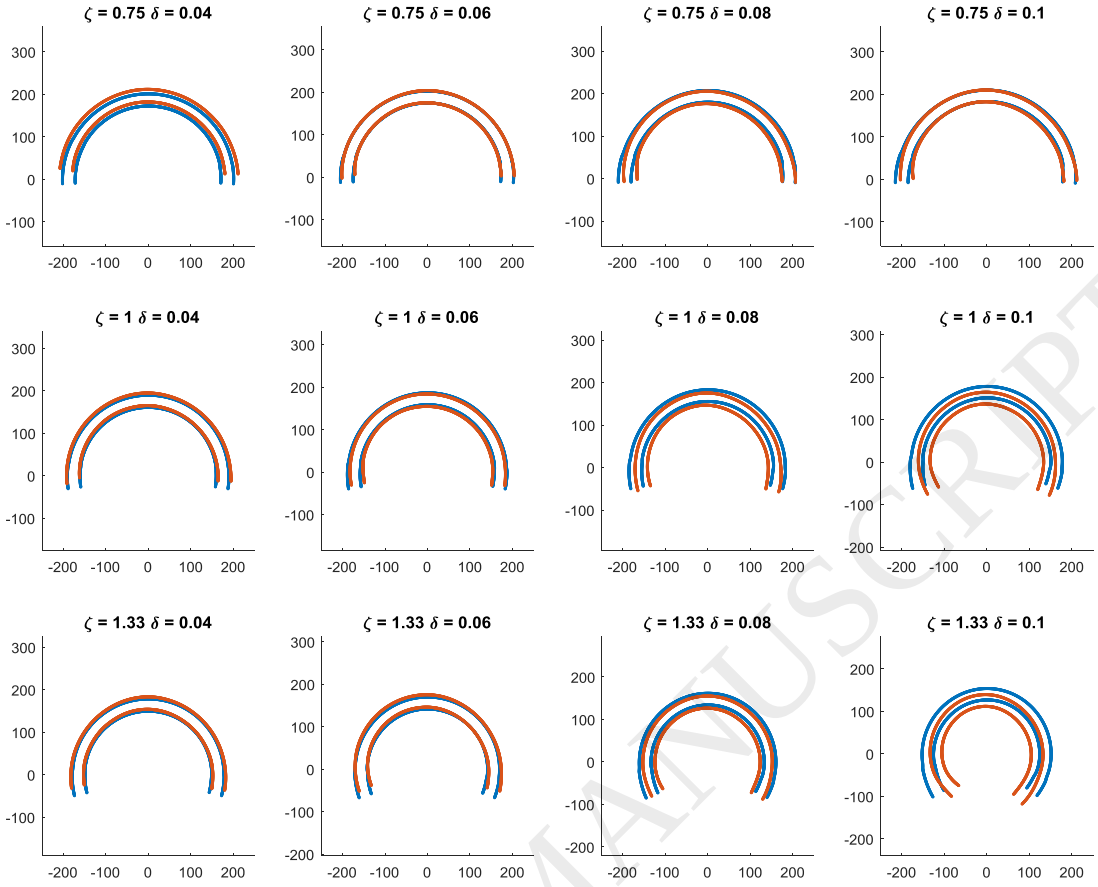

Fig 18 Workpiece outlines for various tool size ratios (ζ) and reductions in thickness (δ). Experiment (Red) vs FEA (Blue)

The complete set of experimental results, FEM and analytical predictions for the medium-wall rings are compared in Fig 19. There is striking agreement between the experiments and both the numerical simulations and analytical predictions over this range of reductions and tool size ratios. Comparing the results at 10% reduction, where the potential for divergence is the largest, the analytical model predicts the radius to within 1.2%, 1.8% and 6.7% of the experimental value for ζ = 0.75, 1.00, and 1.33 respectively. The FEA predicts the same to within 2.2%, 9.8%, 17.3%.

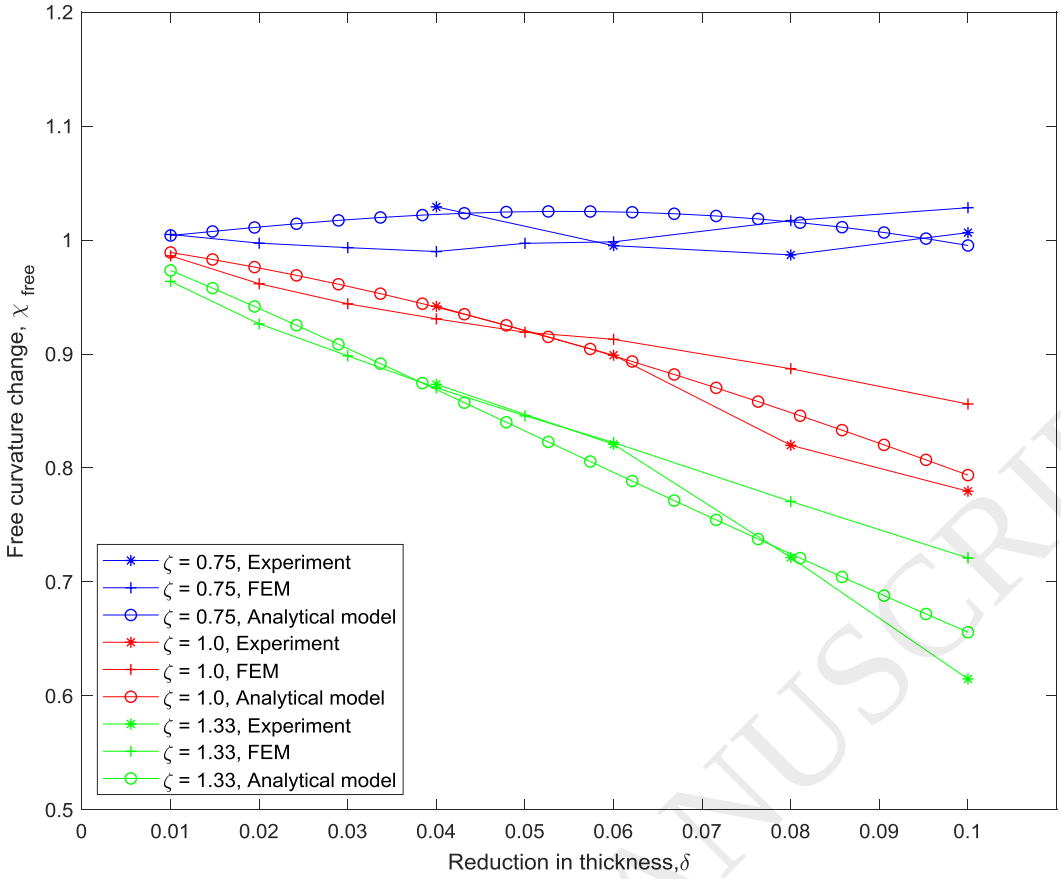

Fig 19 Experiment vs FEM vs Analytical prediction – Medium Walled Rings

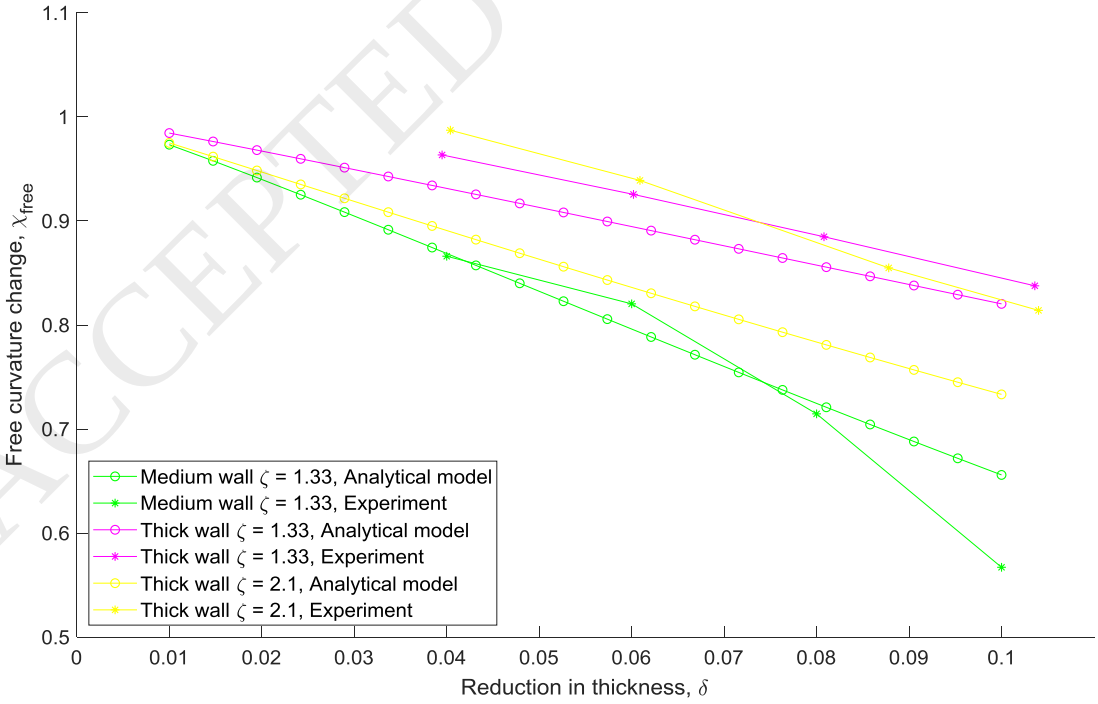

Fig 20 Experiment vs Analytical prediction –Medium and Thick-Walled Rings

The thick wall predictions and results are compared in Fig 20. For the tool size ratio ζ of 1.33 the analytical model accurately predicts the reduced degree of curvature change in the thick-walled case (mauve) compared to the medium wall case (green), with the predicted radii within 3% of the actual radii. This reduced amount of curvature change can be explained by the fact that the model predicts similar differences in circumferential strain, but an even greater amount is required to generate the same curvature change. The model is less effective in the more extreme case of an effective mandrel radius more than twice the forming roll (yellow). Here, the error rises to about 10% although the trend is consistent. Several factors could explain this difference. It could be due to the contribution of shear strain to curvature change; likely to be greatest when the neutral point is shifted the most. Alternatively, it could be due to movement of the centre position of the inlet ring; this increases the clearance between ring and mandrel, reducing its effective radius.

Whereas previous studies of asymmetric strip rolling (e.g. Fig 5 above) showed an oscillatory trend, this is not seen here. It may be that the differences in the mechanical set-up avoids this – the inner tool is not powered, and the support table does not introduce a moment about the plane of the ring (i.e. about the z-axis). The range in reductions in thickness studied here is also smaller, consistent with differing biting-in limits.

2.5.1 Alternative prediction methods

The model proposed in this paper appears adequate for predicting free curvature change under the range of conditions studied. However, it is of interest to explore how well alternative prediction methods would fare.

Two alternatives to the force model used in this paper are considered. The first assumes that the pressure factor at the forming roll and mandrel are equal. The second assumes constant flow stress. The resulting reductions at each roll are used to predict the curvature change as previously.

Fig 21a shows the predictions that result from these assumptions compared to the 'full' model proposed in this paper and the experimental results, for medium-walled rings. In some ways it is remarkable how little difference the choice of force model makes. Indeed, when the effective roll sizes are equal all three predictions converge. The divergence is most visually obvious for roll size ratio 0.75; where the 'full' model gives more accurate results. This is because the full model includes both material hardening and a variable pressure factor (which decreases with increasing contact length), which have an equalising effect for the reductions by making the force at the roll with the largest reduction larger than it would otherwise be. This in turn brings the prediction closer to the green predictions for equal roll size ratio.

For reference Fig 21b plots the resulting predictions for curvature change if Equations 2 and 3, developed for closed rings were to be used. Unsurprisingly neither is well suited to the prediction of open-ended curvature change in lead rings.

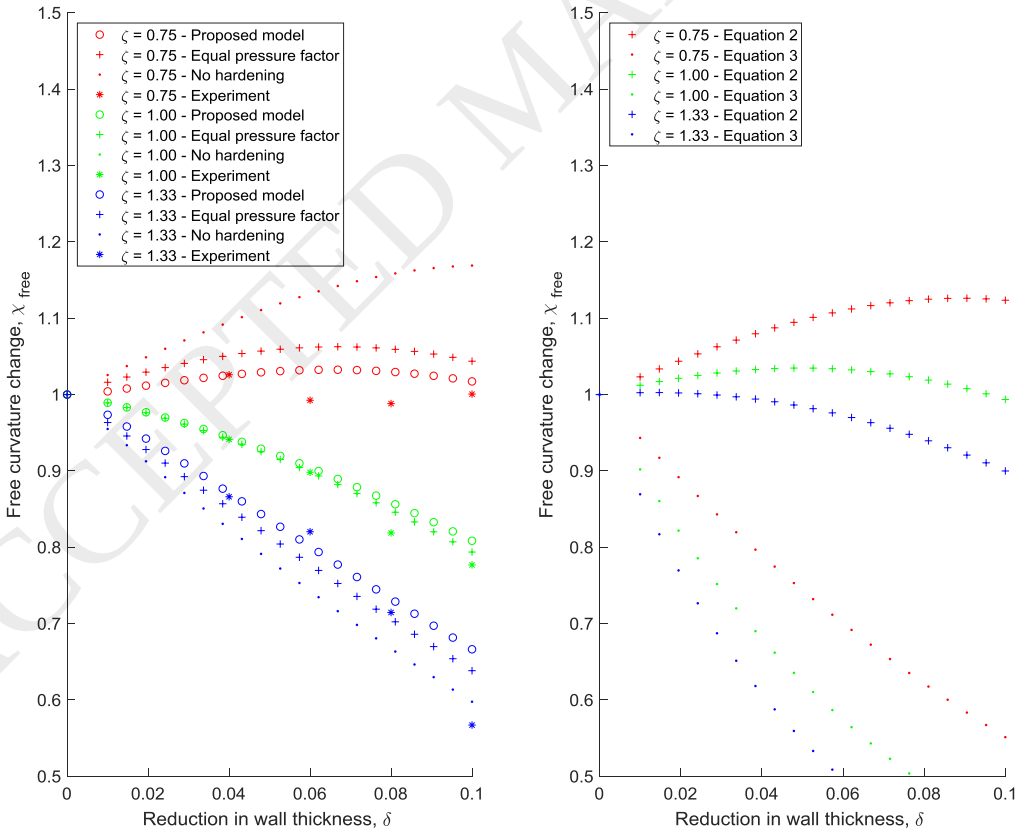

Fig 21 Alternative prediction methods **a.** different force models **b.** direct prediction of reduction

In addition to the analytical model, this section has shown - importantly – that the natural tendency for curvature change in ring rolling may be in opposition to that required in the process. Corrective regulation is needed: the topic of the Section 3.

3 Curvature change in full rings

The previous section established that large curvature changes are possible in the radial roll gap and that the free curvature change may not match the curvature change required to maintain circularity during ring rolling of a full ring. A theory is therefore needed for how the 'correct' curvature changes do occur and thus prevent the process from becoming immediately unstable. In Section 3.1 this paper proposes that elastic moments on the arc of material in the roll-bite provide such a mechanism and a prediction is developed for relationship between applied moment and curvature change. Finally in Section 3.2. a numerical simulation of full ring rolling is carried out to track both changes in curvature, and internal moments around the ring throughout multiple passes. The theories developed in Section 2.1 and Section 3.1 are tested by comparing the FE results to those expected.

3.1 Effect of an end moment on a half ring: 'forced curvature change'

The effect of an end moment on the curvature change of a half-ring workpiece is now considered. Such a moment might arise as a result of a state of self-stress in a full ring or the action of an external guide rolls and could be expected to play a significant role in modifying the change in curvature through the radial roll bite.

3.1.1 Methodology: Forced Curvature Change

The intention of this section is to consider the combined effect of rolling with an externally applied moment on a half ring workpiece – Figure 22a. The inlet and outlet moments were modelled in FEM by applying a moment to two rigid endplates that are in turn connected to the end faces with a tie constraint (Fig 22b). The workpiece is indented and rolled whilst the moment is applied. The moment is then released and the final shape analysed as previously.

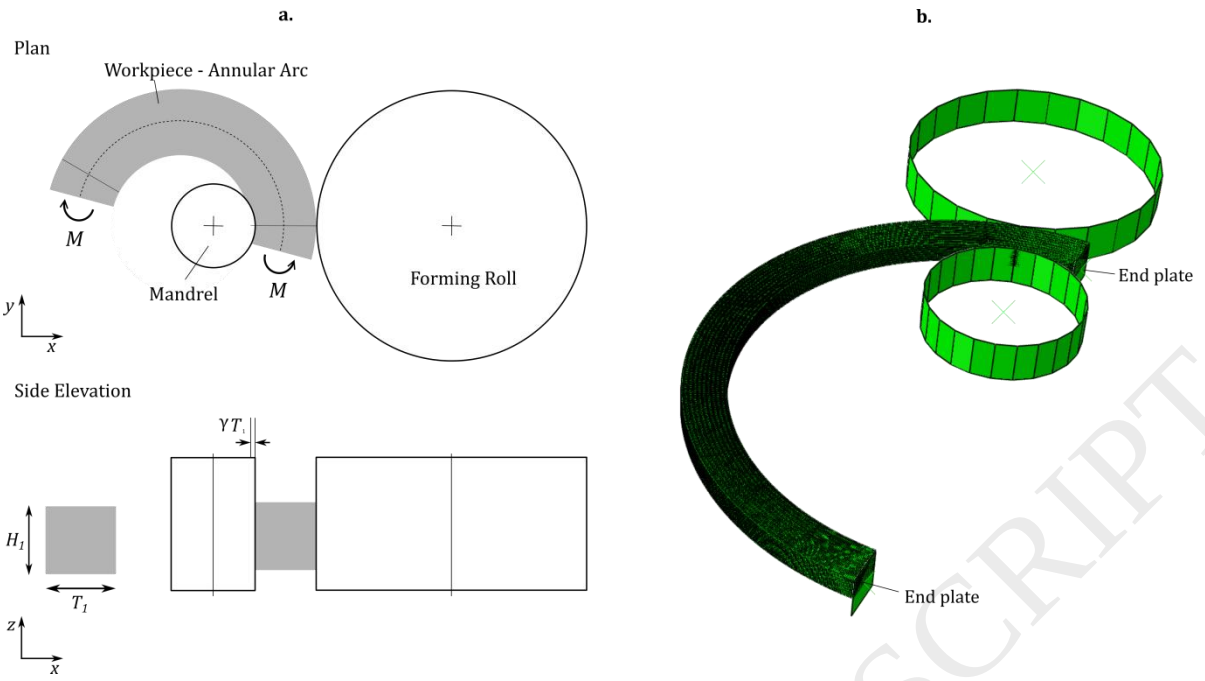

Fig 22 a. Schematic of forced curvature change test **b.** FEM model set-up

The moment is defined positive as in Fig 22a if it 'opens' the ring up. Its value is expressed as a fraction of the moment, M_p, to generate a fully developed plastic hinge, based on the plastic section modulus.:

$$M_p = \frac{HT^2}{4}\overline{\sigma_f} \qquad [23]$$

where for these single-pass trials $\overline{\sigma_f}$ is assumed to be constant, and equal to the initial yield stress (9.3MPa), H is the initial ring height, and T is the initial wall thickness.

The non-dimensional forced curvature change, $T\Delta\kappa_f$ is defined as follows:

$$T\Delta\kappa_f = T(\kappa - \kappa_{free}) \qquad [24]$$

where κ is the actual final curvature, and κ_{free} is the curvature when the moment is zero, and T is the initial wall thickness.

The effect of this moment on curvature change was studied for 3 different reductions in thickness, when the effective tool size ratio, ζ, is 1.33, and for a reduction of 6% with tool size ratios 0.75 and 1.0, as shown in Table 6.

Table 6 'Design of experiments' for forced curvature change FEM simulations

Tool size ratio, ζ	**Reduction in Thickness, δ**	**Applied moment, M/Mp**
0.75	0.06	0.1, 0.2, 0.3
1.0	0.06	0.1, 0.2, 0.3
1.33	0.02, 0.06, 0.10	0.1, 0.2, 0.3

3.1.2 Results: Forced Curvature Change

As expected applying a moment to the arc workpiece during rolling has a strong influence on curvature change. Figure 23 shows the rolled ring outlines for varying reduction in thickness, δ, of 0.02, 0.06 and 0.1 horizontally, and four values of the moment acting on the inlet and outlet vertically – for a specific roll radius ratio (ζ = 1.33). The ratio of outgoing radius to incoming radius ($\overline{R2}/\overline{R1}$) is quoted. Whereas in the free-ended condition (M/M_p=0) the ring curls up, this is reversed as the applied moment increases – even though the value is still significantly less than M_p.

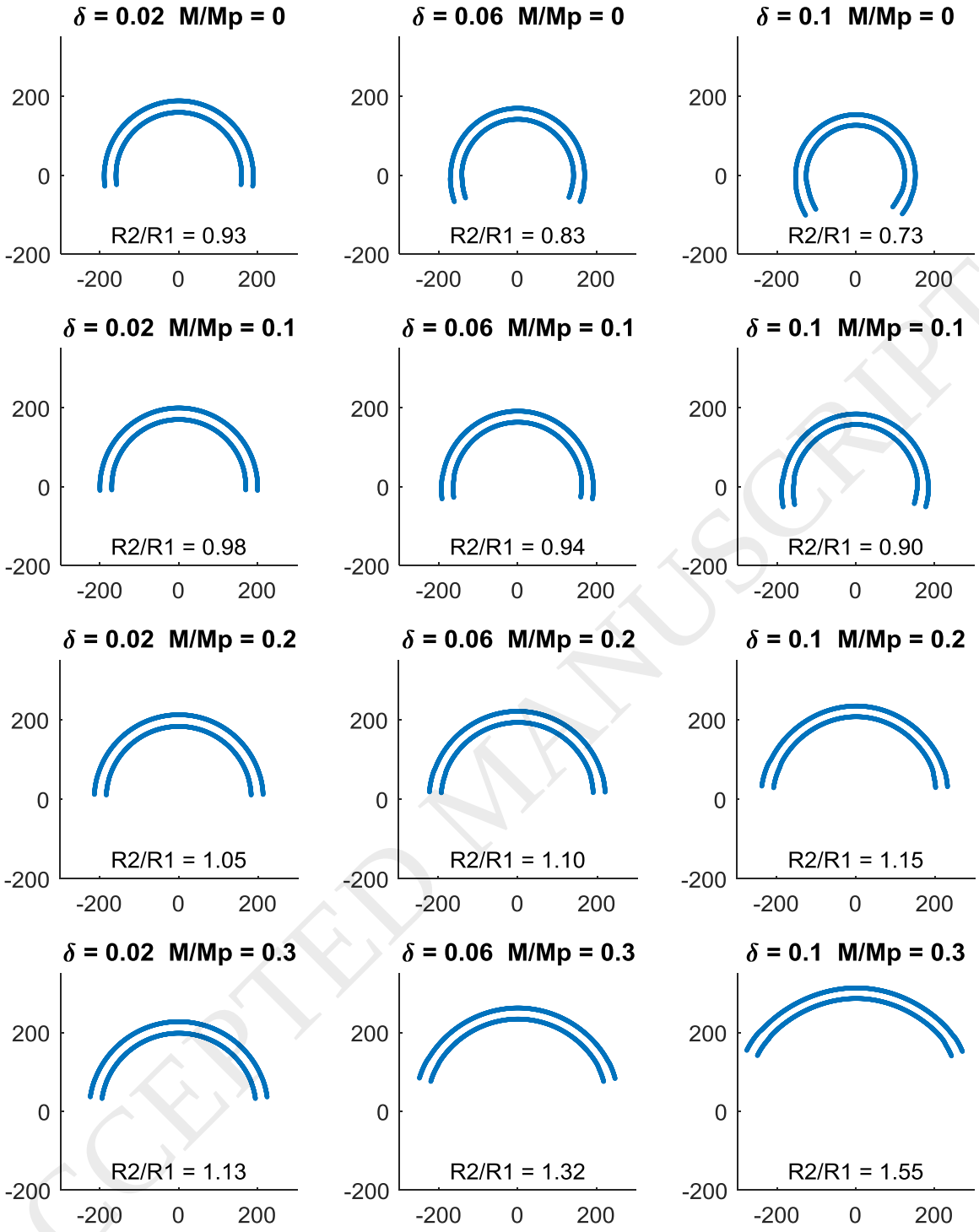

Fig 23 Effect of applied moment on curvature change of rolled half rings, for tool size ratio ζ=1.33, and varying reductions in thickness

There is an almost perfectly *linear* relationship between the applied moment and the change in curvature – see Fig 24a that plots the forced curvature change against the applied

moment for all conditions studied. This is consistent with the stress superposition literature, as will be shown next. The thickness reduction, δ, also plays an important role: on Fig 24a there are three clearly visible linear trendlines, each for a different value of the thickness reduction. As the reduction increases, the amount of curvature change possible (i.e. the slope of the trendline) increases. For a reduction, δ = 0.06, the tool size ratio was also varied. Whereas the tool size ratio strongly influences the free curvature change it is has almost no influence on the additional forced curvature change due to the applied moment.

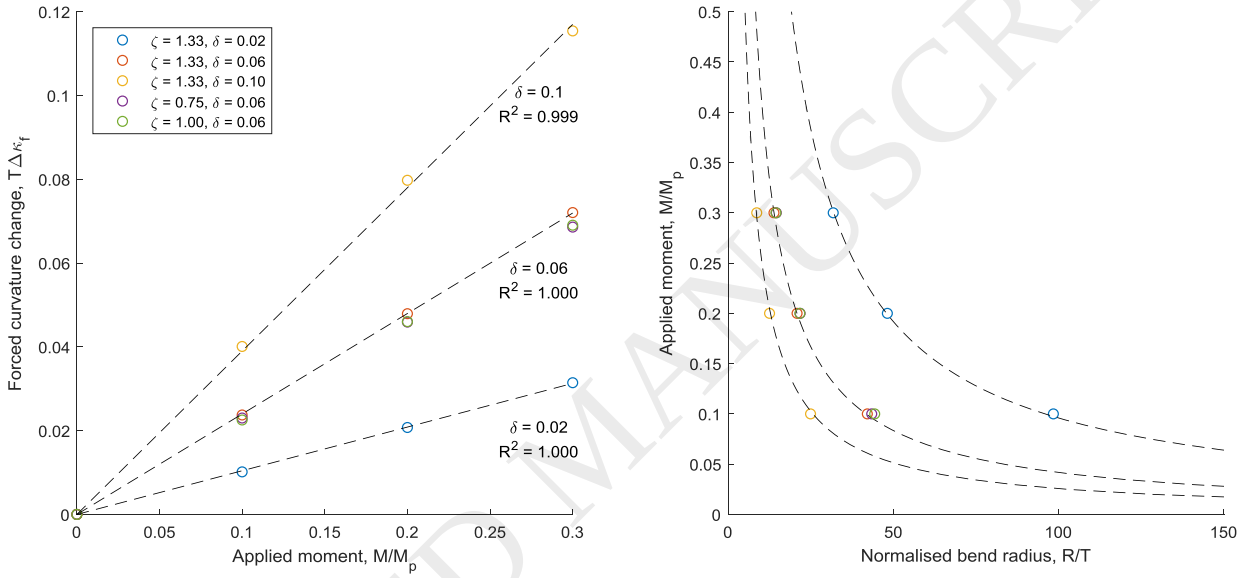

Fig 24 a. Forced curvature change, $T\Delta\kappa_f$ vs Applied moment, M/M_p for different reductions. **b.** M/Mp vs the inverse of $T\Delta\kappa_f$

Figure 24b plots the same information on similar axes to those previously used in the stress-superposition literature (Becker et. al. 2014): the amount of reduction in bending moment from the non-superimposed stress state (M/Mp), is plotted against the inverse of the forced curvature change i.e. the normalised bending radius. This shows explicitly how the reduction in the applied moment increases as 1) the bend radius increases, and 2) the thickness reduction increases.

For the purpose of predicting the value of the internal moment during ring rolling, it will be important to make a prediction for how M/Mp varies with both the amount of forced

curvature change, and the reduction. Here this is done by noting that the gradient of the fitlines in Fig 24a are themselves linearly related to the reduction in thickness, as shown in Fig 25. The agreement is remarkable.

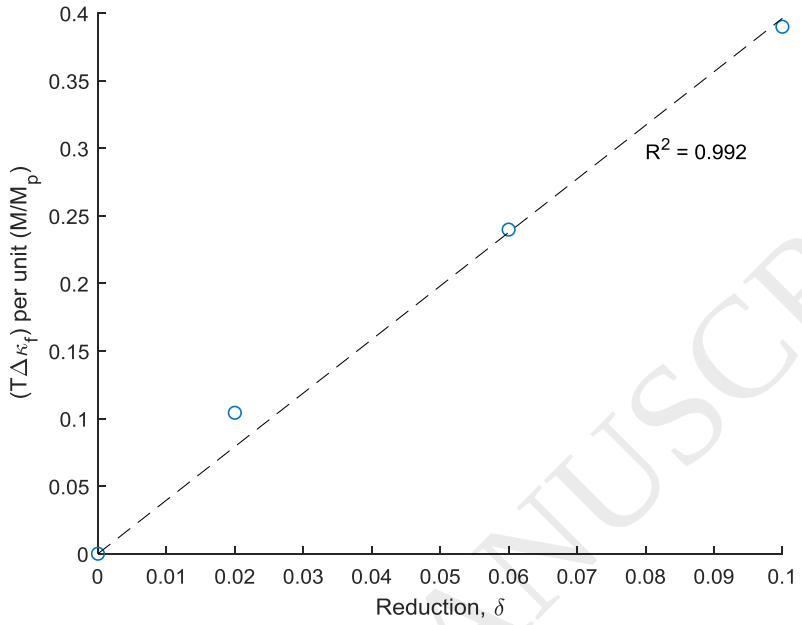

Fig 25 Gradient of the 3 trendlines in Fig 24a vs the reduction in thickness

Using Fig 25, the gradient on Fig 24a is:

$$\mathrm{m} = \alpha_0 \delta \quad \text{where } \alpha_0 = 3.96$$

And therefore, the reduction in the applied M/Mp is almost exactly equal to the ratio of the average circumferential strain induced by bending to the thickness strain:

$$\frac{M}{M_p} = \frac{\Delta\kappa_f T}{\alpha_0 \gamma} \cong \frac{|\varepsilon_c| average}{\varepsilon_T} \qquad [25]$$

In Section 2.5 it was shown that the natural state of curvature change may not match the curvature change required in ring rolling; the above demonstrates this can be corrected by moments in the region of 10-30% of the plastic moment. This value - due to stress superposition - is approximately equal to the ratio of the average circumferential bending strain required to the thickness strain.

3.2 Radial ring rolling of full rings

The previous sub-section showed that the free curvature change in half-ring can be 'corrected' if an elastic moment is applied to its ends. This paper argues that when rolling a full ring a corrective internal bending moment is generated to regulate the curvature change in the radial roll gap. A prediction for this moment is made and tested against a numerical simulation.

3.2.1 Prediction of the internal bending moment

A prediction for the internal bending moment acting at the radial roll zone during radial only rolling is built up based on the results of 2.5 and 3.1.

By volume conservation – assuming no height growth – the required new curvature, κ_2, for a given reduction in thickness, δ, is simply:

$$\kappa_2 = \kappa_1(1-\gamma) \qquad [26]$$

where κ_1 is the initial curvature.

The free (radius of) curvature change is calculated as described in Fig 7, so that the free curvature is:

$$\kappa_{free} = \frac{1}{\chi_{free}}\kappa_1 \qquad [27]$$

The forced curvature change required is then:

$$\Delta\kappa_f = \kappa_2 - \kappa_{free} = \kappa_1\left(1-\gamma-1/\chi_{free}\right) \qquad [28]$$

By using Equation 25 above, the predicted internal bending moment is:

$$\frac{M}{M_P} = \frac{T\kappa_1\left(1-\gamma-1/\chi_{free}\right)}{\alpha_0\gamma} \qquad [29]$$

As an illustration, Fig 26 plots the predicted internal bending moment against the reduction in thickness for different tool size ratios.

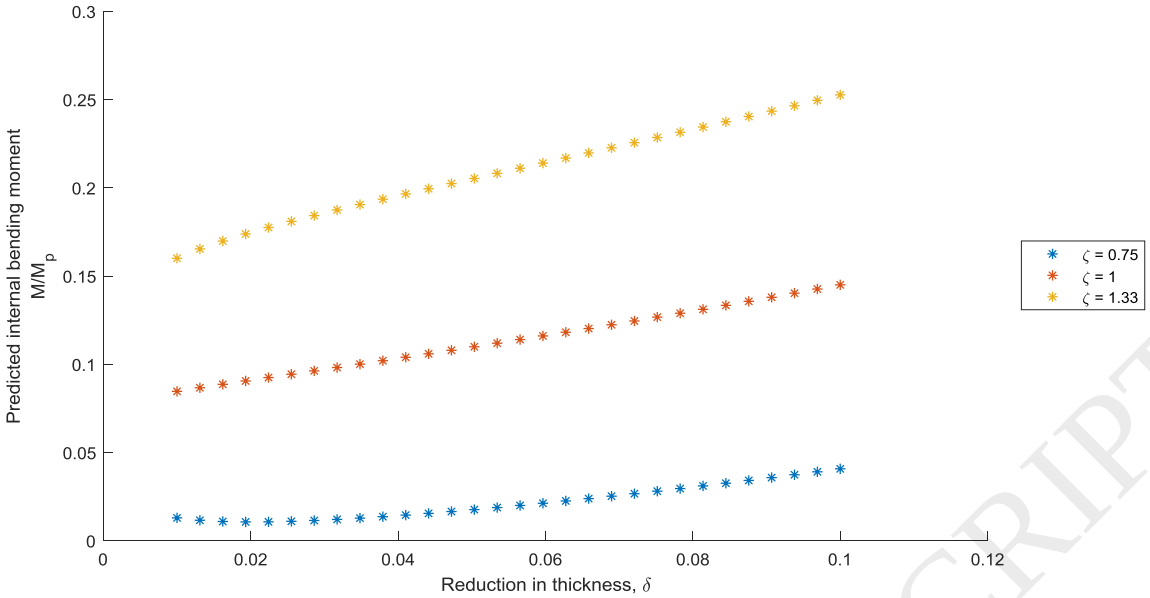

Fig 26 Predicted bending moment against reduction in thickness for different tool size ratios, ring slenderness $\bar{R}$/T = 6.3, strain hardening coefficient, n=0.17

3.2.2 FEM of radial ring rolling

The understanding of curvature change developed in this paper, and in particular the prediction for the internal bending moment is tested against a 3D FEM simulation.

A radial ring rolling process with no guide rolls is considered. It is expected that there will be curvature changes both across the radial roll gap (as investigated here), and in the outer ring region as investigated by Johnson and Needham (1968). The predicted internal bending moments at the radial roll bite are expected to develop as a state of self-stress due to bending of the outer ring.

A 3-D FEM simulation was made as shown in Fig 27. Two rotations of the ring were considered. In the simulation the radial roll gap was initially equal to the starting ring wall thickness. The forming roll then rotated at constant velocity and the mandrel moved with constant velocity so that at the end of the first ring rotation, the specified wall thickness reduction was achieved. On the second rotation of the ring the mandrel moved with a slightly reduced constant velocity so the thickness strain across the roll gap remained approximately constant throughout the second revolution.

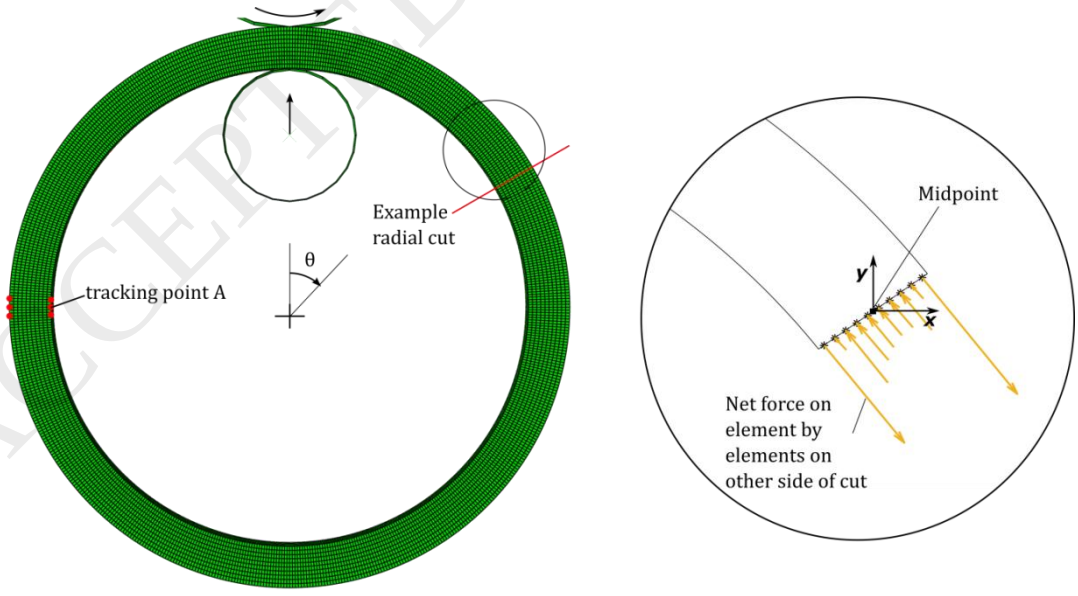

Fig 27 FEM set-up radial only rolling of a full ring

The mesh consists of 48,000 elements spread around the full ring circumference. All other parameters are as previously stated.

The local average radius of curvature was measured at 600 points around the ring circumference. This was done by fitting a circle to 3 corresponding points on both the outer and inner surfaces, each spaced 3 nodes apart circumferentially, and taking the mean value. To reduce noise the resulting curvature was filtered with a moving average filter averaging across the neighbouring 10 ring points. Tracking point A – indicated on Fig 27 - initially 90° from the roll bite was used to report the change in curvature over time.

The internal bending moment was also measured at each nodal point around the ring, using a radial cut. The internal bending moment was calculated by summing along the line of elements to one side of the cut the force on each element due to element on the other side of the cut (using the ABAQUS variable NFORC) multiplied by the distance from the midpoint:

$$M = \sum_i Fx_i * y_i - Fy_i * x_i \qquad [30]$$

Five simulations were carried out at different tool size ratio, and reduction as set out in Table 7.

Table 7: 'Design of Experiments' for Radial ring rolling of a full ring FEM

Tool size ratio	**Reduction per pass**
0.75	6%
1.0	6%
1.33	2%, 6%, 10%

3.2.3 Results

The curvature and equivalent plastic strain about a particular material point (marked A in Fig 27) are plotted in Fig 28 for all the FEM simulations. On the left column (a), three different

tool size ratios are compared, for the same reduction. On the right (Fig 28b), three different reductions are compared for the same tool size ratio.

In all cases tracking point A passes the radial roll gap twice; first after ¼ of a revolution and then after 1¼ revolutions. At this point in time the plastic strain (lower graphs) increases rapidly, and – particularly on the second pass through the roll gap - there is a jump in radius of curvature. Whilst the point is in the roll gap, the outer and inner surfaces conform to the shape of the rollers and the curvature is undefined.

The curvature history is very similar between the different tool size ratios (Fig 28a): this is to be expected since unlike previously the constraint of the rest of the ring must enforce an increase in the radius of curvature as the circumferential length extends. The only indication that something different is happening shows in the total equivalent plastic strain, measured for the inner most element. The strain is highest in the case where the mandrel is smallest, as was previously shown for a half ring.

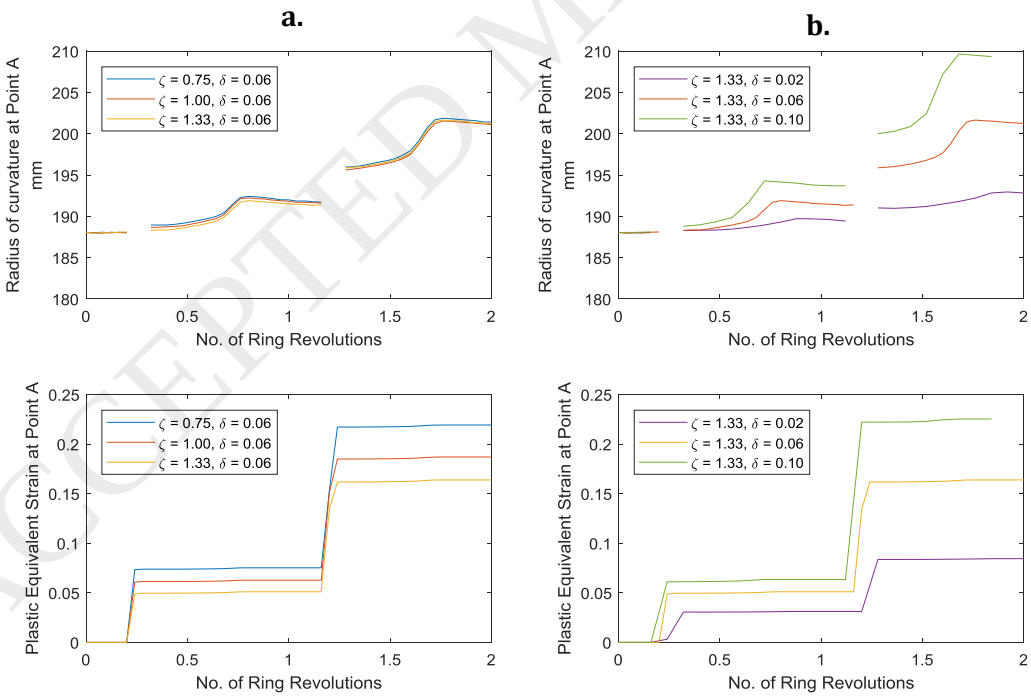

Fig 28 Curvature and plastic strain about tracked point A on the ring with **a.** RM/RF=0.75,1.0,1.33 and δ = 0.06 **b.** RM/RF=1.33 and δ = 0.02, 0.06, 0.10

The preceding work predicted that - despite very similar curvature history - there should be significantly different internal stresses between the different tool size ratios. Fig 29 reveals this through a series of diagrams showing the end loading on the arc of material in the radial roll gap at the end of the first revolution. In the left hand column, the reduction is constant (0.06) and the tool size ratio varies (0.75, 1.00, 1.33) from top to bottom. Here, when the mandrel is smallest, the bending moment is actually negative: it 'curls up' the ring. At tool size ratio 1.0 and 1.33 the bending moment is progressively larger. The value of the plastic moment, Mp, at this point is 57.8 Nm, based on the section size of the incoming material.

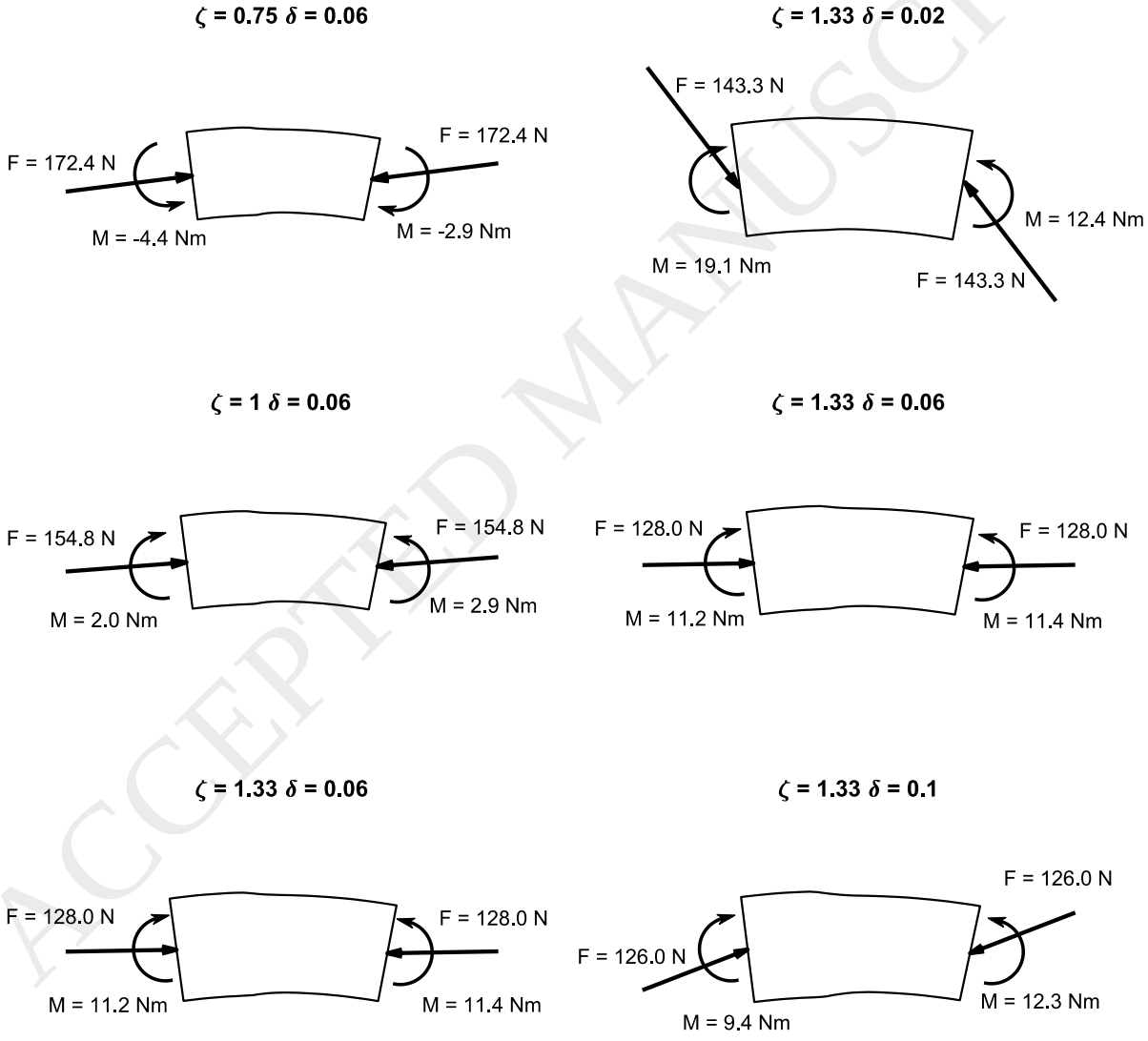

Fig 29 Diagram showing resultant end forces and moments on the arc of material in the radial roll zone at the end of the first revolution for **a.** RM/RF=0.75,1.0,1.33 and δ = 0.06 **b.** RM/RF=1.33 and δ = 0.02, 0.06, 0.10

The forces and moments have been checked for equilibrium. They should be in equilibrium because the rest of the ring has no other external loading on it. The difference in the value of the incoming and outgoing moment is the product of the 'axial' force and distance between their lines of action which are parallel but not collinear.

The diagrams reveal a second feature: in addition to the bending moment there is a significant compressive force on the arc in the rollbite. The presence of such a force was predicted by Hawkyard et al. (1973) who argued its magnitude should be sufficient to generate a plastic hinge opposite the roll gap, allowing the outer ring to accommodate the incompatibility caused by rolling. This is shown in Fig 30: the bending moment rises sinusoidally to a maximum value in each case of M/Mp approximately equal to 1. Returning to Fig 28 this explains the change in curvature outside the rollgap region, some of which is recovered elastically.

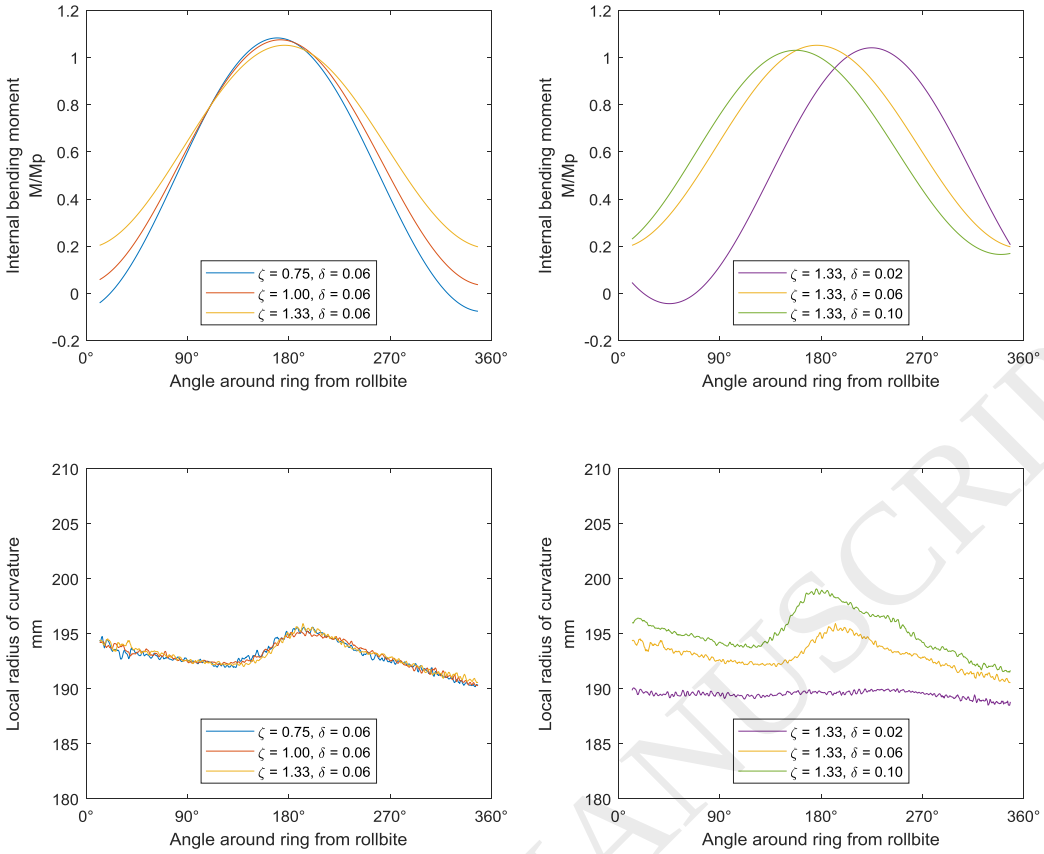

Fig 30 Bending moment and Local radius of curvature at the end of the first revolution for **a.** RM/RF=0.75,1.0,1.33 and δ = 0.06 **b.** RM/RF=1.33 and δ = 0.02, 0.06, 0.10

Figure 31 shows a filtered value of the moment at the roll bite as the rolling proceeds. The moment quickly builds up from zero as the reduction increases to reach a quasi-steady value. The average value of the moment during the second revolution is plotted with a dashed line. The unsteadiness in the values may reflect the unsteady nature of the process of radial rolling without guide rolls, with the ring likely to 'rock' from side to side e.g. as discussed by Fourozan et. al. (2003). The rocking shows up in the simulation data: the minimum x coordinate of the workpiece (left to right on Fig 27) oscillates with an amplitude of approximately 1mm, whereas the minimum y coordinate (up and down) decreases smoothly.

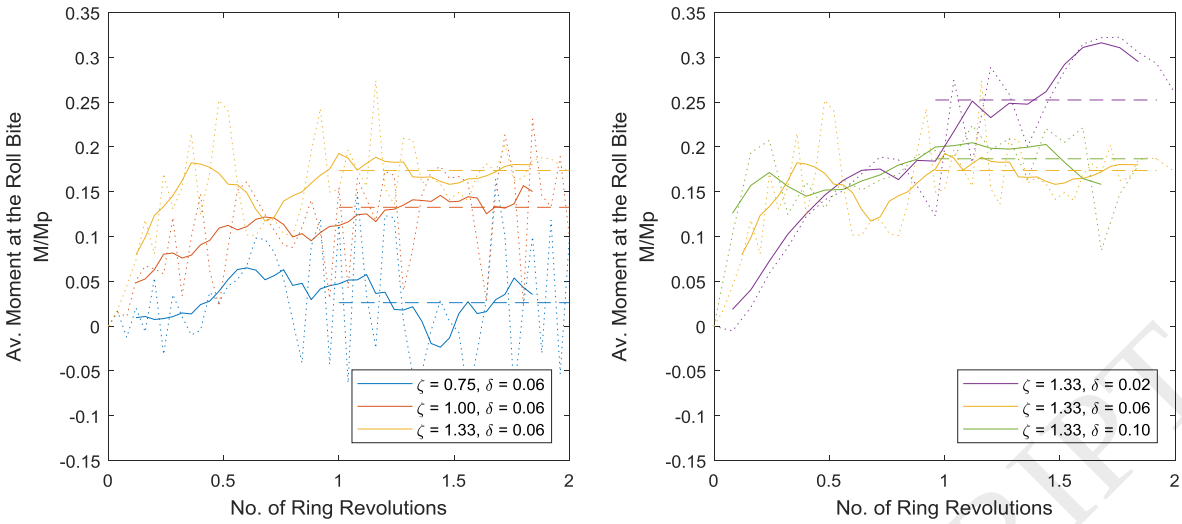

Fig 31 Bending moment at the Roll Bite against time for **a.** RM/RF=0.75,1.0,1.33 and δ = 0.06 **b.** RM/RF=1.33 and δ = 0.02, 0.06, 0.10

The internal bending moment predicted by Equation 29 is compared with these average values observed in the FEM – see Fig 32. There is reasonable agreement throughout when δ=0.06. For tool size ratios ζ=0.75 and 1.00 the prediction is lower than the simulated result by 24% and 14% respectively. For ζ=1.33 the predicted result is higher by 19%. However, whereas the prediction is for a slight upward trend as the reduction increases, the largest value of moment occurs when the reduction is the smallest (δ=0.02). Interestingly this also corresponds to the case where the axial force is the least 'horizontal' and may be the least effective at 'opening' the ring up, requiring larger curvature changes in the radial roll gap.

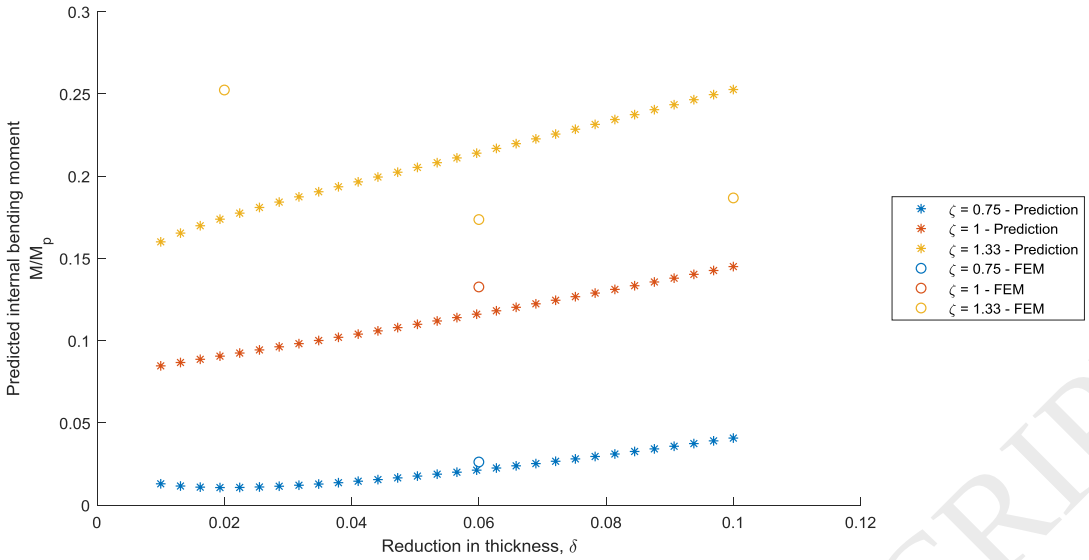

Fig 32 Bending moment at the Roll Bite: analytical prediction vs FEM

4 Discussion and conclusions

This study has explored the previously tacit knowledge that in radial ring rolling the workpiece curvature changes as it passes through the roll gap. Literature to date on curvature change in ring rolling is sparse and only explicitly considered for changes in curvature in the region outside of the roll gap, so this work provides a significant step forward in understanding.

Furthermore, it has been shown that the 'jumps' in curvature are often achieved in opposition to the natural tendency for the roll gap to 'curl up' the ring. The roll size ratio and reduction have been shown to strongly influence this 'free curvature change'. The paper has shown that elastic moments acting on the workpiece provide a corrective mechanism.

In addition this paper has introduced analytical methods to predict each of these effects without the need for time-consuming numerical simulations: a model of the free curvature change was put forward based on force equilibrium. A prediction was made for the value of the corrective moment, inspired by stress-superposition theory. The former has been verified against a set of experimental trials and FEM simulations, and the latter shown to have predictive power against FEM simulations of radial ring rolling.

The work has a number of wider implications for ring rolling. In cases where loss of circularity is common, such as for thin-walled rings (e.g. Gellhaus, 1999) it may provide useful guidance over both tool sizing and force limits/settings for guide rolls. Roll sizing is constrained by multiple factors including tool strength, their influence over the maximum reduction and spread patterns. This work offers a new rationale for designing the roll sizes that may be important in certain applications.

To do this, the free curvature model of this paper could be applied repeatedly to search for the mandrel size that results in the 'correct' change in radius. Fig 31 illustrates this, showing how the 'ideal' size would vary throughout an example ring rolling process in which the radius increases and wall thickness reduces. The ideal mandrel is sensitive to the clearance between

the inner radius and the mandrel, which changes significantly during the early stages of this process. The ideal radius is then more stable as the radius grows and wall thickness reduces. The reduction has a limited influence. It would be impractical to change the mandrel size throughout the process and so a process designer might select a mandrel radius to match the 'ideal' radius towards the end of the process when the ring is least stiff.

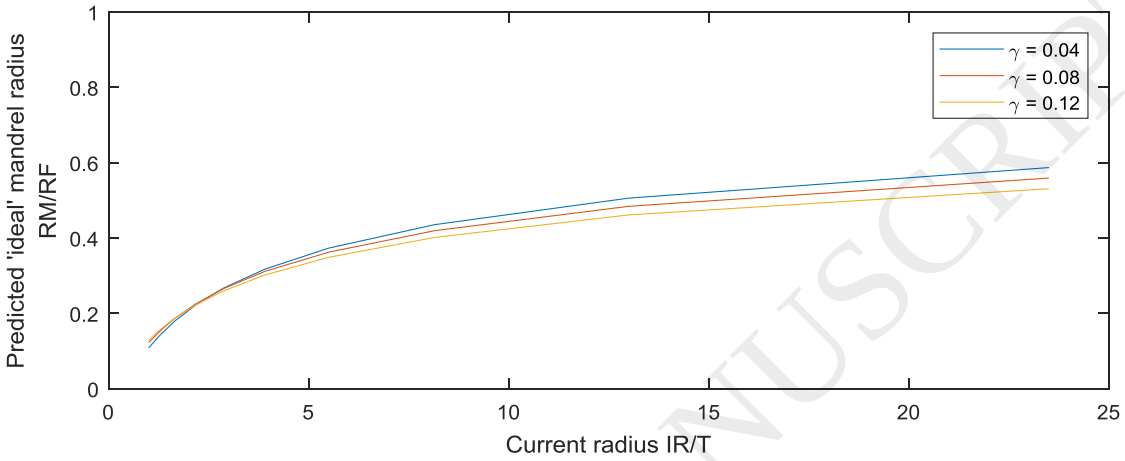

Fig 33 Change in the 'Ideal' Mandrel Radius against the Inner Radius. Calculated for the case of a ring of initial inner radius 175 mm, wall thickness 125 mm, and forming roll radius 200mm

A second avenue this work opens up is the positioning of the guide rolls: if the natural tendency is often for the ring to 'curl up', it would be interesting to explore the effect of placing the guide rolls inside the ring rather than outside it. For instance for thin-walled rings with known stability problems, it would be valuable to investigate how stability is affected by guide roll placement. A knock-on benefit of a marginal reduction in the roll force may be achieved if sufficient hoop-wise tension is developed.

The following conclusions are drawn:

- Curvature changes in radial ring rolling are the combined result of plastic curvature changes in the radial roll bite, and bending in the rest of the ring which are both elastic and plastic

- The free curvature change for a half ring is strongly influenced by the relative sizes of the tools. For a 10% thickness reduction there was respectively a radius increase of 3%, -22% and -39% for effective mandrel radii 75%, 100% and 133% of the forming roll.
- The free curvature change is affected by the thickness reduction: this amplifies the change in curvature. In one case examined, for a 4% reduction the radius change was -13% and for a 10% reduction it was -39%.
- This paper proposes a model for free curvature change by applying force equilibrium to each roll – an extension of Hawkyard et al. (1973)'s work. For tool size ratios 0.75-1.33, reductions from 2-10%, and two different ring thicknesses, it predicted the outgoing radius to within 7%.
- The forced curvature change varies linearly with the applied internal bending moment, and the reduction in the moment for a given curvature change is approximately equal to the average circumferential bending strain to thickness strain.
- In radial ring rolling an internal bending moment of between 0-25% of the plastic moment – varying with the tool size ratio - is seen at the inlet and outlet to the roll bite whose value is predicted to within 25% by the analytical modelling developed in this paper.

Acknowledgments

The authors' work was supported by the UK Engineering and Physical Sciences Research Council under [EP/N02351X/1 and EP/K018108/1]. The authors are grateful for the contributions and suggestions provided by members of the Use Less Group, in particular Dr. Johannes Lohmar.

References

Becker, C., Tekkaya A. E., Kleiner, M., 2014 . Fundamentals of the incremental tube forming process. CIRP Annals – Manufacturing Technology. 63 pp. 253-256

Christiansen, P., Martins, P. A. F., Bay N., 2016. Friction Compensation in the Upsetting of Cylindrical Test Specimens. Experimental Mechanics. 56/6 pp. 1271-1279

Cleaver, C. J., 2016. The development of an incremental ring rolling process with axial and circumferential constraints. PhD Thesis. University of Cambridge

Cleaver, C. J., Allwood, J. M., 2017 Incremental profile ring rolling with axial and circumferential constraints. CIRP Annals – Manufacturing Technology , 66. pp 285-288

Collins, I. F., Dewhurst, P., 1975. A slipline field analysis of asymmetrical hot rolling. Int. J. Mech Sci 17/10 pp. 643-651

Euro Forge. 2018. Production Figures. http://www.euroforge.org/statistics/production-figures.html

Forouzan, M. R., Salmi, M., Gadala, M. S., Aljawi, A. A., 2003. Guide roll simulation in FE analysis of ring rolling. J. Materials Processing Technology, 142. pp 213-223

Gellhaus, M., 1999. Technische Informationen 2/99, Radial-Axial Ringwalzen-Millenium Edition, SMS Eumuco GmbH Produktionbereich Wagner Banning Ringwalzen

Hawkyard, J. B., Johnson, W., Kirkland, J., Appleton, E., 1973. Analyses for roll force and toque in ring rolling, with some supporting experiments. Int. J. mech. Sci. 15. pp 873-893

Hua, L., Deng, J., Qian, D., Lan, J., Long, H., 2016. Modelling and application of ring stiffness condition for radial-axial ring rolling. Int. J. Machine Tools and Manufacture, 110. pp. 66-79

Jenkouk, V., Hirt, G., Franzke, M., Zhang, T., 2012 Finite element analysis of the ring rolling process with integrated closed-loop control. CIRP Annals – Manufacturing Technology 61 pp. 267-270

Johnson, W., Needham, G., 1966 Further experiments in asymmetrical rolling. Int. J. Mech Sci 8/6 pp. 443-455

Johnson, W., Needham, G., 1968. Plastic hinges in ring indentation in relation to ring rolling. Int. J. Mech Sci 10/6 pp 487-488

Koppers, U., Kopp, R., 1992 Geometry of the forming zones in ring rolling. Steel research international 63/2 pp. 74-77

Li L., Yang, H., Guo, L., Sun, Z., 2008. A control method of guide rolls in 3D-FE simulation of ring rolling. J Materials Processing Technology 205:99–110

Minton, J., Brambley, E., 2017. Meta-analysis of curvature trends in asymmetric rolling. Procedia Engineering 207 pp. 1355-1360

Parvisi, A., Abrinia, K., Salimi, M., 2011. Slab analysis of Ring Rolling assuming constant shear friction. Journal of Materials Engineering and Performance. 20(9):1505-1511

Schmidt, J., Haessner, F., 1991. Recovery and recrystallization of high purity lead determined with a low temperature calorimeter. Scripta Metallurgica et Materialia 25/4 pp 969-974

Salimi, M., Sassani, F., 2002. Modified slab analysis of asymmetrical plate rolling. Int. J. Mech Sci 44 pp 1999-2023

Shivpuri, R., Chou, P. C., Lau, C. W., 1988. Finite element investigation of curling in non-symmetric rolling of flat stock. Int. J. Mech Sci. 30/9 pp 625-635

List of Figures

Fig 15 FEM model assembly set-up

Fig 16 Experimental results for free curvature change in ring rolling of half rings for various tool size ratios (ζ) and reductions in thickness (δ)

Fig 17 Comparison of free curvature change for medium-walled and thick-walled half rings, with tool size ratio ζ = 1.33 and 2.12, varying the reduction in thickness (δ)

Fig 18 Workpiece outlines for various tool size ratios (ζ) and reductions in thickness (δ). Experiment (Red) vs FEA (Blue)

Fig 19 Experiment vs FEM vs Analytical prediction – Medium Walled Rings

Fig 20 Experiment vs Analytical prediction –Medium and Thick-Walled Rings

Fig 21 Alternative prediction methods a. different force models b. direct prediction of reduction

Fig 22 a. Schematic of forced curvature change test b. FEM model set-up

Fig 23 Effect of applied moment on curvature change of rolled half rings, for tool size ratio ζ=1.33, and varying reductions in thickness

Fig 24 a. Forced curvature change, $T\Delta\kappa f$ vs Applied moment, M/Mp for different reductions. b. M/Mp vs the inverse of $T\Delta\kappa f$

Fig 25 Gradient of the 3 trendlines in Fig 24a vs the reduction in thickness

Fig 26 Predicted bending moment against reduction in thickness for different tool size ratios, ring slenderness $\bar{R}/T = 6.3$, strain hardening coefficient, n=0.17

Fig 27 FEM set-up radial only rolling of a full ring

Fig 28 Curvature and plastic strain about tracked point A on the ring with a. RM/RF=0.75,1.0,1.33 and δ = 0.06 b. RM/RF=1.33 and δ = 0.02, 0.06, 0.10

Fig 29 Diagram showing resultant forces and moments on the arc of material in the radial roll zone at the end of the first revolution for a. RM/RF=0.75,1.0,1.33 and δ = 0.06 b. RM/RF=1.33 and δ = 0.02, 0.06, 0.10

Fig 30 Bending moment and Local radius of curvature at the end of the first revolution for a. RM/RF=0.75,1.0,1.33 and δ = 0.06 b. RM/RF=1.33 and δ = 0.02, 0.06, 0.10

Fig 31Bending moment at the Roll Bite against time for a. RM/RF=0.75,1.0,1.33 and δ = 0.06 b. RM/RF=1.33 and δ = 0.02, 0.06, 0.10

Fig 32 Bending moment at the Roll Bite: analytical prediction vs FEM

Fig 33 Change in the 'Ideal' Mandrel Radius against the Inner Radius. Calculated for the case of a ring of initial inner radius 175 mm, wall thickness 125 mm, and forming roll radius 200mm

List of Tables

Table 1 Variables fixed in this study

Quantity	Description	Value used in this study
$\overline{R1}/_{T1}$	Ring slenderness	188 mm /30 mm = 6.26
$\dot{\bar{\varepsilon}}$	Thickness strain rate	0.2 / s
$H1/_{T1}$	Blank aspect ratio	30 mm / 30 mm = 1.0
$R_{FR}/_{T1}$	Forming roll radius to wall thickness ratio	100 mm / 30 mm = 3.33

Table 2 Flow curve fit to the model $\bar{\sigma}=K\varepsilon^n$ for $\dot{\bar{\varepsilon}} = 0.2/s$ in region $\varepsilon = 0\text{-}0.2$

Parameter	Value
K	33.1
n	0.17

Table 3 Parameters used in the Finite Element Simulation

Feature	**Details**
Contact	Exponential contact: • 500MPa @ 0.00mm clearance • 0 MPa @ 0.02 mm clearance Coulomb friction, μ = 0.3 Contact stabilization: • Stabilization factor: 0.01 • Clearance at which stabilization is zero: 0.05mm • Factor at end of rolling phase: 0
Material Model	Young's modulus: 50MPa Tabulated plastic flow curve at strain rates: • 0, 0.01/s, 0.1/s, 0.2/s, 1/s • as per Fig 13
Workpiece	Element type: C3D8R (8 node brick with reduced integration) Mesh size: 600 circumferential x 10 radial x 8 axial = 48,000 elements
Tools	Analytical rigid bodies

Table 4 Sensitivity of the free curvature change, χ_free, to the friction coefficient, μ. FEM simulation with tool size ratio, ζ=1.0 and 1.33, and reduction, δ=0.08

Friction coefficient	ζ=1.0	ζ=1.33
	χ_{free}	χ_{free}
0.2	0.91	0.79
0.25	0.90	0.78
0.3	0.89	0.77
0.35	0.89	0.78
0.40	0.89	0.78

Table 5 'Design of experiments' for free curvature change experiments and FEM

Ring sizing	Tool size ratio, ζ	Reduction in thickness, δ	
		Experiments	FEM
IR = 173 mm OR = 203 mm H = 30 mm	0.75 (R_M = 39.0, R_F = 100)	0.04, 0.06, 0.08 & 0.10	0.01, 0.02, 0.03, 0.04, 0.05, 0.06, 0.08 & 0.10
	1.00 (R_M = 48.3, R_F = 100)	0.04, 0.06, 0.08 & 0.10	0.01, 0.02, 0.03, 0.04, 0.05, 0.06, 0.08 & 0.10
	1,33 (R_M = 58.9, R_F = 100)	0.04, 0.06, 0.08 & 0.10	0.01, 0.02, 0.03, 0.04, 0.05, 0.06, 0.08 & 0.10

Table 6 'Design of experiments' for forced curvature change FEM simulations

Tool size ratio, ζ	**Reduction in Thickness, δ**	**Applied moment, M/Mp**
0.75	0.06	0.1, 0.2, 0.3
1.0	0.06	0.1, 0.2, 0.3
1.33	0.02, 0.06, 0.10	0.1, 0.2, 0.3

Table 7: 'Design of Experiments' for Radial ring rolling of a full ring FEM

Tool size ratio	**Reduction per pass**
0.75	6%
1.0	6%
1.33	2%, 6%, 10%